

Hard X-ray Emission From Low Mass X-ray Binaries

D. Barret, J. F. Olive & L. Boirin

Centre d'Etude Spatiale des Rayonnements, CNRS/UPS, 9 Avenue du Colonel Roche, 31028 Toulouse Cedex 04, F
 Didier.Barret@cesr.fr

C. Done

Department of Physics, University of Durham, South Road, Durham DH1 3LE, England, UK
 chris.done@durham.ac.uk

G. K. Skinner

School of Physics and Astronomy, University of Birmingham, Edgbaston, Birmingham B15 2TT, UK
 gks@star.sr.bham.ac.uk

J. E. Grindlay

Harvard Smithsonian Center for Astrophysics, 60 Garden Street, Cambridge, MA 02138, USA
 josh@head-cfa.harvard.edu

ABSTRACT

We report on *Rossi X-ray Timing Explorer* observations of four type I X-ray bursters; namely 1E1724–3045, GS1826–238, SLX1735–269 and KS1731–260. The first three were in a low state, with 1–200 keV X-ray luminosities in the range $\sim 0.05\text{--}0.1 L_{\text{Edd}}$ (L_{Edd} : Eddington luminosity for a neutron star = 2.5×10^{38} ergs s^{-1}), whereas KS1731–260 was in a high state with a luminosity $\sim 0.35 L_{\text{Edd}}$. The low state sources have very similar power spectra, displaying high frequency noise up to ~ 200 Hz. For KS1731–260, its power spectrum is dominated by noise at frequencies $\lesssim 20$ Hz; in addition a quasi-periodic oscillation at 1200 Hz is detected in a segment of the observation. The 1–200 keV spectra of the low state sources are all consistent with resulting from thermal Comptonization with an electron temperature (kT_{E}) around 25–30 keV. For KS1731–260, the spectrum is also dominated by thermal Comptonization, but with a much lower $kT_{\text{E}} \sim 3$ keV and no significant hard X-ray emission. With the exception of GS1826–238, there is an underlying soft component, carrying at most $\sim 25\%$ of the total 1–200 keV luminosity. For all sources, we have detected an iron $K\alpha$ line at 6.4 keV (although it is weak and marginal in 1E1724–3045). A reflection component is present in the spectra of GS1826–238 and SLX1735–269, and for both we find that the reflecting medium subtends only a small solid angle ($\Omega/2\pi \sim 0.15, 0.28$). The origin of the line and the reflection component is most likely to be irradiation of the accretion disk by the X-ray source.

We suggest a model in which the region of main energy release, where hard X-rays are produced would be an optically thin boundary layer merged with an Advection Dominated Accretion Flow (ADAF), and would be responsible for the rapid variability observed. The soft component observed probably represents the unscattered emission from an optically thick accretion disk of variable inner radius. When the accretion rate increases, the inner disk radius shrinks and the strength of the reflected component and associated iron line increase. At the same time, the Comptonization region cools off in response to an increased cooling flux from the accretion disk and from the reprocessed/reflected component, thus leading progressively to a quenching of the hard X-ray emission. If low state NSs accrete via ADAFs, the observation of X-ray bursts, indicating that all the accreting matter actually accumulates onto the NS surface, argues against the existence of strong winds from such accretion flows.

Finally, we discuss two criteria recently proposed to distinguish between non-quiet Black Holes (BHs) and Neutron Stars (NSs), and that are not contradicted by existing observations. The first one states that when thermal Comptonization is responsible for the hard X-ray emission, only BHs have kT_{E} larger than ~ 50 keV. However, this criterion is weakened by the fact that there are NSs displaying non-attenuated power laws extending up to at least 200 keV, possibly implying non-thermal Comptonization or thermal Comptonization with kT_{E} larger than 50 keV. The second criterion stipulates that only BHs are capable of emitting hard X-ray tails with 20–200 keV luminosities $\gtrsim 1.5 \times 10^{37}$ ergs s^{-1} .

1. Introduction

It is now well established that hard X-ray emission ($E \gtrsim 30$ keV) from X-ray binaries is not exclusively associated with Black Hole systems (BHs). The major breakthrough came with the SIGMA and BATSE observations, which provided the first unambiguous detections of type I X-ray bursters (hence Neutron Star systems, NSs) at ~ 100 keV (Barret & Vedrenne 1994, Barret & Tavani 1997 and references therein). However, due to the moderate sensitivity and low spectral resolution of these instruments and the lack of simultaneous X-ray observations, it was impossible to investigate the conditions under which NSs emit hard X-rays. Similarly, very little could be inferred about the accretion geometry and the relative contribution of the potential emitting regions to the total emission (NS surface, boundary layer, accretion disk, corona). In addition, the hard X-ray data alone were not good enough to discriminate between the thermal and non-thermal models that have been put forward to account for this emission. Finally, if the emission of hard X-rays is indeed common to BHs and NSs, there may remain some differences either in the shape of the hard tails (position of the energy cutoff; e.g. Tavani & Barret 1997, Churazov et al. 1995), or in the luminosities that can be radiated simultaneously in soft and hard X-rays¹ (Barret et al. 1996, Van Paradijs & Van der Klis 1994, Barret & Vedrenne 1994, Zhang et al., 1996). All these potential differences have yet to be quantified precisely. They can now be addressed through observations performed by the *Beppo-SAX* and the *Rossi X-ray Timing Explorer* (RXTE) satellites; the latter combining the Proportional Counter Array (PCA) and the High Energy X-ray Timing Experiment (HEXTE) (Bradt et al. 1993). These two instruments offer for the first time the possibility of observing NSs with good sensitivity and excellent timing capabilities simultaneously from 2 to ~ 150 keV.

In this paper, we report on the RXTE observations of four type I X-ray bursters; namely 1E1724–3045, GS1826–238, SLX1735–269 and KS1731–260. All these sources have in common that they have already been detected up to ~ 100

¹In this paper, we define soft X-rays, as photons with energy between 1 and 20 keV (also X-rays), and hard X-rays, as photons with energy between 20 and 200 keV.

keV at least once (Barret & Tavani 1997). The analysis has been made in a coherent way for all sources to allow a reliable and consistent comparison of their respective properties. The paper is organized as follows. First we review the relevant spectral observations of the four sources, and present their long term RXTE All Sky Monitor (ASM) light curves (Sect 2). We then describe our data reduction scheme, before presenting the results of our RXTE pointed observations (Sect 3). In section 4, we discuss the main features of our timing and spectral results and their implications for our understanding of NS accretion. Finally, we discuss the most recent observational criteria that have been proposed to distinguish non-quiescent BHs and NSs on the basis on their broad band spectral properties.

2. The sources

First, let us review briefly the previous observations of these four sources. We will emphasize X-ray spectral observations, in particular previous N_H measurements relevant to the PCA spectral analysis, existing hard X-ray observations, and finally more general information about these sources.

2.1. 1E1724–3045

1E1724–3045 is the most extensively studied of the four sources discussed here. It is located in the globular cluster Terzan 2 in the general direction of the Galactic center. Its distance was first estimated to be 7.7 kpc (Ortolani et al. 1997), and recently revised to 6.6 kpc (Barbuy et al. 1998). It is a weakly variable X-ray source, and a persistent, though variable, hard X-ray source (Goldwurm et al. 1993, 1994). Details about previous X-ray observations can be found in Barret et al. (1999a). Broad band spectral observations have already been performed by *Beppo-SAX* (Guainazzi et al. 1998). They showed that the 1 to 200 keV spectrum could be well fitted by the sum of a soft and a hard Comptonized component. The former could be equally fitted by a single temperature blackbody (BB) of $kT_{BB}=0.6$ keV, $R_{BB}=12$ km, or a Multi-Color Disk blackbody (MCD, Mitsuda et al. 1984) with $kT_{in}=1.4$ keV, $R_{in}\sqrt{\cos\theta}=2.7$ km (at 10 kpc corresponding to $R_{in}\sqrt{\cos\theta}=2.0$ km at 6.6 kpc). The hard Comptonized compo-

ment was fitted with a *Comptt* model (Titarchuk 1994) with an electron temperature of ~ 27 keV, an optical depth ~ 3.3 for a spherical scattering cloud, and a temperature of 0.6 keV (kT_W) for the seed photons. The ratio of the bolometric (0.1-100 keV) luminosity of the soft component to the total luminosity was 11% and 36% for the BB and MCD models respectively. However, as pointed out by Guainazzi et al. (1998), whereas the radius derived from the BB fit is close to the NS radius, the very small value inferred for R_{in}^2 appears unphysical (for any plausible values of the source inclination); hence the hypothesis that the soft component comes from the boundary layer around the NS might be preferred.

An ASCA observation confirmed the hardness of the source in X-rays, and allowed an accurate determination of N_{H} towards the source ($\sim 1.2 \times 10^{22}$ H atoms cm^{-2}). This value is consistent with that expected from the optical reddening of the cluster (Barret et al., 1999a).

²The MCD model returns kT_{in} and $R_{\text{in}}\sqrt{\cos\theta}$ (for an assumed distance), which are the color temperature of the inner accretion disk and the projected inner disk radius (note that in the case of a pseudo-newtonian disk with zero-stress inner boundary conditions around a Schwarzschild BH, the actual inner disk radius is 2.73^{-1} times less than the measured R_{in} , see Gierlinski et al. 1999). Correction for spectral hardening must be made to kT_{in} and R_{in} to account for the fact that the inner disk opacity is dominated by electron scattering. We use a spectral hardening factor $f=1.7$, a value consistent with the source luminosity (Shimura & Takahara 1995), and determine the effective temperature as $kT_{\text{eff}}=kT_{\text{in}}/f$, and the effective inner disk radius as $R_{\text{eff}}=f^2 R_{\text{in}}=2.9 R_{\text{in}}$. For 1E1724-3045, this means that $kT_{\text{eff}}=0.82$ keV, $R_{\text{eff}}=11.4$ km for an assumed inclination angle of 60° (the source is not a dipper, therefore its inclination must be less than 75°). If we further assume that the disk terminates at the last stable orbit, then as described in Ebisawa et al. (1994), R_{S} (the Schwarzschild radius) is related to R_{eff} as $3R_{\text{S}} \approx 9 M_{\text{NS}} \text{ km} \propto \frac{3}{5}\eta R_{\text{eff}}$ (M_{NS} mass of the neutron star in units of M_{\odot} , $\eta < 1$ accounts for the decrease of $R_{\text{in}}\sqrt{\cos\theta}$ by relativistic effects, see Ebisawa et al. 1994, here we take $\eta = 0.6$ as in Shimura & Takahara (1995)). From this, the low inferred value of R_{eff} implies a very low mass of $0.4 M_{\odot}$ for the NS (for a $1.4 M_{\odot}$ NS, R_{eff} should be 37 km, equivalent to $R_{\text{in}} \sim 13$ km). This does not seem to favor the MCD model used to fit the soft component in the *Beppo-SAX* data of 1E1724-3045. However, one has to keep in mind that R_{in} is derived from the normalization of the MCD model, and therefore would be underestimated if some fraction of the disk flux is scattered in a corona. The measured value of R_{in} derived from the unscattered fraction would then depend on the geometry, and the optical depth of the scattering corona.

2.2. GS1826-238

When GS1826-238 was discovered serendipitously by GINGA in 1988, it was first classified as a transient source, and further classified as a Black Hole Candidate (BHC) based on its rapid and intense flickering and hard Power Law (PL) spectrum in X-rays (Tanaka 1989). The source was later detected by TTM (In't Zand 1992), ROSAT-PSPC (Barret et al. 1995a), and at hard X-ray energies by OSSE (Strickman et al. 1996). The BH nature of GS1826-238 was questioned (e.g. Strickman et al. 1996, Barret et al. 1996), but the firm evidence that GS1826-238 did not contain a BH came with the discovery of type I X-ray bursts (the unmistakable signature of a NS) with the *Beppo-SAX* Wild Field Cameras (WFC, Ubertini et al. 1997). In the WFC data, the 70 bursts observed over more than 2.5 years of source monitoring exhibit a quasi-periodicity of 5.76 hours in their occurrence times (Ubertini et al. 1999). In addition, the so-called α parameter which is the ratio between the average persistent X-ray flux to the average flux emitted during X-ray bursts (assuming that both are isotropic) was estimated to be 60 ± 7 for two of the 70 bursts analyzed by Ubertini et al. (1999). Similarly In't Zand et al. (1999), using also a sample of two bursts, observed $\alpha = 54 \pm 5$ consistent with the previous estimate. This value is consistent with a picture in which all the accreting material is accumulated onto the NS and helium is burned during the bursts (α should be ~ 20 and ~ 80 for pure Hydrogen and Helium burning respectively).

As is the case for 1E1724-3045, broad band observations of GS1826-238 already exist. First, Strickman et al. (1996), combining non simultaneous GINGA (X-ray) and OSSE (hard X-ray) data showed that the 2-200 keV spectrum of the source could be fitted by an exponentially cutoff power law (CPL: $\Gamma = 1.76 \pm 0.02$, $E_{\text{Cutoff}} = 58 \pm 5$ keV, Γ is the photon index of the power law, i.e. the energy index would be $\Gamma-2$) with a weak (and marginally significant) reflection component. More recently, *Beppo-SAX* observed the source, following a BATSE trigger which indicated that GS1826-238 was emitting hard X-rays (Frontera et al. 1998, Del Sordo et al. 1999). The 0.5-200 keV spectrum was well fitted by a composite model consisting of a blackbody of 0.94 ± 0.05 keV, and a PL of photon index $\Gamma = 1.34 \pm 0.04$,

exponentially cutoff at 49 ± 3 keV. The column density measured by *Beppo-SAX* was 0.47×10^{22} H atoms cm^{-2} , consistent with the ROSAT PSPC value ($0.5 \pm 0.04 \times 10^{22}$ H atoms cm^{-2} , Barret et al. 1995); both being slightly larger than the value expected from the optical reddening towards the source ($E(B-V) \sim 0.4$ corresponding to 0.22×10^{22} H atoms cm^{-2} , Predehl & Smith 1995, Barret et al. 1995). Another *Beppo-SAX* observation performed half a year before by In't Zand et al. (1999) yielded best fit spectral parameters consistent with those reported in Del Sordo et al. (1999).

GS1826–238 has a $V = 19.1 \pm 0.1$ optical counterpart (Barret et al. 1995, Homer et al. 1998) in a possible 2.1 hour orbital period system, and is therefore a Low Mass X-ray Binary (LMXB). If the 2.1 hour modulation is the true orbital period of the system, one can try to estimate the source distance following the approach of Van Paradijs & McClintock (1994). In LMXBs, the bulk of the optical light originates from the reprocessing of the X-rays in the accretion disk. For systems for which reliable distance estimate exists, there is a good correlation between the absolute V magnitude and the X-ray luminosity (L_X) and the size of the accretion disk (and hence the orbital period P_{orb} , $L_V \propto L_X^{1/2} P_{\text{orb}}^{2/3}$). Most LMXBs have M_V in the range 0-2, whereas some short period systems have M_V in the range 3-5. With a 2.1 hr orbital period, GS1826–238 is a short period system, and if one assumes M_V in the above range (and an absolute dereddened V magnitude of 17.9), one gets a formal distance range between ~ 4 and ~ 10 kpc. Constraints on the source distance can also be inferred from the observation of X-ray bursts. In't Zand et al. (1999) derived an unabsorbed bolometric peak flux of a burst of $2.7 \pm 0.5 \times 10^{-8}$ ergs $\text{s}^{-1}\text{cm}^{-2}$. The fact that this burst did not show evidence for photospheric expansion implies that its luminosity is below the Eddington limit (L_{Edd}) which we assume to be 2.5×10^{38} ergs s^{-1} (this value is appropriate for helium-rich material, a $1.4 M_{\odot}$ NS, and a moderate gravitational redshift correction, Van Paradijs & McClintock 1994). This in turn implies an upper limit on the source distance of 9.6 kpc. In the remainder of this paper, we assume a distance of 7 kpc for GS1826–238.

2.3. SLX1735–269

SLX1735–269 was reported for the first time in 1985, when it was detected by the *Spacelab 2* X-ray Telescope (Skinner et al. 1987). However, it was present in the Einstein Slew Survey in observations performed ~ 5 years earlier (Elvis et al. 1992). SLX1735–269 was later detected by TTM (In't Zand 1992), by ART-P, ROSAT-PSPC (Grebenev et al. 1996) and ASCA (David et al. 1997). SIGMA observations have shown that it is a persistent hard X-ray source of the Galactic center region (Goldwurm et al. 1996). The weakness of the source (~ 15.4 mCrab in the 35-75 keV range) did not allow tight constraints to be put on the time averaged (1990-1994) hard X-ray spectrum, which could be fitted either by a simple PL of photon index $\Gamma \sim 2.9 \pm 0.3$, or alternatively by a Comptonization model (*Compst* in XSPEC, Sunyaev and Titarchuk, 1980) with kT_{E} of 26_{-9}^{+35} keV (Goldwurm et al. 1996). Although early suspected to contain a NS based on the softness of its hard X-ray spectrum (Goldwurm et al. 1996), its nature remained uncertain until type I X-ray bursts were discovered with the *Beppo-SAX* WFC (Bazzano et al. 1997). The ASCA observations of SLX1735–269 revealed that its 0.6-10 keV spectrum could be well fitted with a PL of index 2.15 (David et al. 1997), absorbed through an N_{H} of $\sim 1.4 - 1.5 \times 10^{22}$ H atoms cm^{-2} , a value which is consistent with a source location near the Galactic center (i.e. at a distance of ~ 8.5 kpc, David et al. 1997). The N_{H} value derived with ASCA is also consistent with the one derived from the ROSAT-PSPC and ART-P observations ($1.2 - 1.4 \times 10^{22}$ H atoms cm^{-2} , Grebenev et al. 1996). The rapid variability of the source was recently investigated by Wijnands & Van der Klis (1999), using a short 10 kilosecond *Rossi X-ray Timing Explorer* observation performed between February and May, 1997 (see below).

No accurate distance estimate exists so far. From the burst reported in Bazzano et al. (1997a) (1.5×10^{-8} ergs $\text{s}^{-1}\text{cm}^{-2}$, 2-10 keV, Bazzano et al. 1997b), an upper limit of ~ 10 kpc can be derived (after bolometric corrections and assuming a blackbody of 2 keV for the burst). In the remainder of the paper, we will assume a distance of 8.5 kpc.

2.4. KS1731-260

KS1731-260 was discovered in October 1988 by TTM (Sunyaev et al. 1990), and then classified as a transient. KS1731-260 is located in the Galactic center region, about 5° away from the Galactic nucleus and only 1° from the X-ray pulsar GX1+4. Above the mean persistent level of 80 mCrab (2.7×10^{-10} ergs $s^{-1} cm^{-2}$, 1-20 keV), TTM observed several X-ray bursts from KS1731-260, thus indicating that it contains a weakly magnetized NS. The TTM spectrum was fitted by a Thermal Bremsstrahlung (hereafter TB³) of 5.7 keV, absorbed through an N_H of 2.2×10^{22} H atoms cm^{-2} . Follow-up ROSAT and optical observations indicated that the source is a likely LMXB (Barret et al. 1998). The N_H derived from the ROSAT-PSPC all sky survey observations of 1.3×10^{22} H atoms cm^{-2} for a PL fit; is about a factor of 2 less than the value derived with TTM, thus possibly indicating intrinsic N_H variations within the source. More recently, we observed KS1731-260 with ASCA (September 27th, 1997) and confirmed the N_H found by ROSAT (Narita et al. 1999). Additional X-ray observations can be found in Yamauchi & Koyama (1990) and Aleksandrovich et al. (1995). KS1731-260 was detected only once in hard X-rays between 35 and 150 keV by SIGMA, and has remained undetectable since then at these energies (Barret et al. 1992). Unfortunately, no simultaneous X-ray observations exist for the SIGMA detection.

RXTE first observed KS1731-260 in July-August 1996. It was then in its standard high state. These observations led to the discovery of a highly coherent 524 Hz periodic X-ray signal at the end of the contraction phase of an X-ray burst that showed photospheric expansion (Smith et al. 1997). This signal was tentatively interpreted as an indication of the NS spin (Smith et al. 1997). However, in the same data set, two simultaneous High Frequency Quasi-Periodic Oscillations (HFQPOs) at 898 ± 3.3 Hz and 1158 ± 9 Hz were

³Note that at such luminosities, TB fits are unphysical because they imply emission measures $10^{59} - 10^{60}$ cm^3 . The optically thin requirement leads to a size of $10^{10} - 10^{11}$ cm for the cloud. These sizes are at least $\sim 100 - 1000$ times larger than the region of main energy release around a NS. This means that one should be cautious about the N_H fitted, because its value depends critically on the shape assumed to fit the continuum.

also found (Wijnands & Van der Klis 1997), see below). The frequency separation (260.3 ± 9.6 Hz, corresponding to 3.8 msec) which is equal to half the frequency of the burst oscillations was then interpreted as the true NS spin frequency (Wijnands & Van der Klis 1997).

In addition, assuming that the burst observed by RXTE reached the Eddington luminosity, a distance of 8.8 ± 0.3 kpc was derived for the source (Smith et al. 1997). At this distance, the implied source X-ray luminosity at the time of the RXTE observations was 5.7×10^{37} ergs s^{-1} . Finally a N_H of 6×10^{22} H atoms cm^{-2} was derived for a TB fit of the RXTE PCA spectrum; a high value, significantly larger than the ASCA, ROSAT and TTM ones.

2.5. ASM light curves

The RXTE ASM long term light curves of all four sources are shown in Fig. 1 (for information about the RXTE/ASM see Levine et al. 1996). The mean ASM count rates are 2.9 cts s^{-1} (~ 38 mCrab), 2.9 cts s^{-1} (~ 38 mCrab), 2.6 cts s^{-1} (~ 35 mCrab), 11.3 cts s^{-1} (~ 150 mCrab) in the 2-12 keV range for 1E1724-3045, GS1826-238, SLX1735-269 and KS1731-260 respectively. Assuming a PL spectrum of photon index 2, and the source N_H , at the source distance, these values correspond to average 1-20 keV luminosities of $\sim 1.0 \times 10^{37}$ ergs $s^{-1} = 0.04 L_{Edd}$, 8.8×10^{36} ergs $s^{-1} = 0.03 L_{Edd}$, 1.3×10^{37} ergs $s^{-1} = 0.05 L_{Edd}$ for 1E1724-3045, GS1826-238 and SLX1735-269 respectively. For KS1731-260, assuming a thermal-like X-ray spectrum, the mean flux is about a factor of 5 larger: $\sim 4.9 \times 10^{37}$ ergs $s^{-1} = 0.2 L_{Edd}$. These light curves provide the first confirmation of the low variability of SLX1735-269, GS1826-238 and 1E1724-3045. In particular, for GS1826-238, this together with independent measurements (e.g. Barret et al. 1995; In't Zand et al. 1999) indicate that since its discovery in 1988, the source is a very stable accretor, and certainly not a classical transient as previously thought. The light curve of KS1731-260, shows also that the source is persistent but occasionally undergoes low intensity states, which might be associated with episodes of hard X-ray emission.

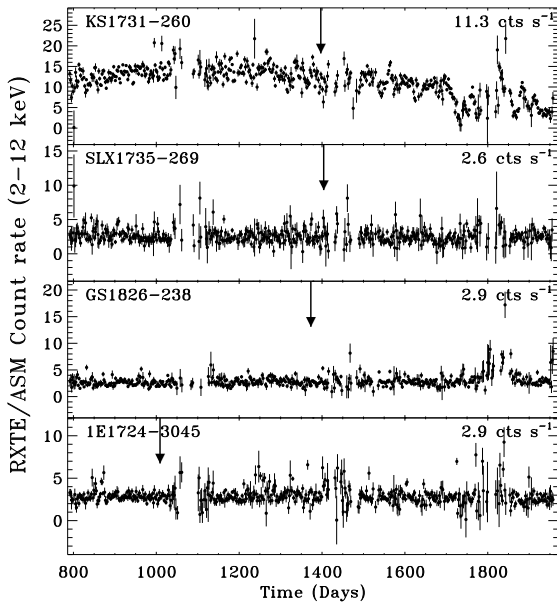


Fig. 1.— The RXTE/ASM long term light curves of 1E1724–3045, GS1826–238, SLX1735–269 and KS1731-260. Time is given as days after January 1st, 1994. Data have been selected using *fselect* to satisfy the criterion that the measured rate for each individual “dwell” is positive and that the reduced χ^2 of the fit to recover the source intensity is less than 1.5. Data from all three Scanning Shadow Cameras are combined within *lcurve*. The binning time of the light curves is 2 days. The gaps in the light curves are due to the sun getting too close to the source region (see Levine et al. 1996 for information about the ASM). The dates of our pointed observations are indicated with arrows.

3. Observations and Results

The PCA instrument consists of a set of 5 identical Xenon proportional counters covering the 2–60 keV energy range with a total area of about 6500 cm² (Bradt et al. 1993). The HEXTE instrument is made of two clusters of 4 NaI(Tl)/CsI(Na) phoswich scintillation detectors providing a total effective area of 1600 cm² in the 15–200 keV range⁴ (Rothschild et al. 1998). The two clusters rock

⁴Note that this is about a factor of 4 larger than the effective area of the SIGMA imaging telescope for a source located in its fully coded field of view (Paul et al. 1991).

alternately between the source and background fields to measure the background in real time. Special care has been taken to avoid the presence of any known X-ray sources in the background fields.

The rapid variability of the 4 sources has been investigated with the PCA *science event* data. Our spectral analysis is based on the *standard 2* data for the PCA. They provide count spectra each 16 seconds in 128 energy channels covering the 2 to 100 keV range. The FTOOLS used for PCA background estimation is *pcabackest* version 2.1b (released in October 1998). For HEXTE, we also use the standard mode data. They provide 64 channel count spectra each 16 seconds. PCA spectra have been first accumulated for each PCU units for integration times varying from ~ 1000 to ~ 2000 seconds, roughly equivalent to an orbit after filtering for good time intervals. In particular, PCA data recorded during and up to 30 minutes after the SAA passage have been removed using the FTOOLS 4.2 version of *xtfilt*. PCA response matrices were then computed for each PCU using the FTOOLS *pcarsp 2.36*. We have then summed individual PCU spectra using *addspec* version 1.0.1, which combines not only the PHA files, but also the background PHA files, and computes the associated response matrices.

For HEXTE, spectra were accumulated for each cluster with similar integration times to those used for the PCA. The latest response matrices have been used (*hexte_97mar20c_pwa.rm*). Cluster A and B spectra were then combined together using *addspec*, to get a single HEXTE spectrum averaged over the whole observation. The source and background light curves and spectra were corrected for deadtime effects using version 0.0.1 of *hatedead*.

Version 10.00 of XSPEC (Arnaud 1996) has been used for the spectral fitting. When combining PCA and HEXTE spectra, the energy ranges of the fit were 2.5 to 25 keV for the PCA, and above 25 keV and up to at most 150 keV for HEXTE. These energy ranges were selected to exclude the steepening of the PCA spectrum above 25 keV (in most spectra, it starts around 20 keV), as well as the flatening of the HEXTE spectrum towards low energies. Starting at 2.5 keV with the PCA implies that in most cases, the N_H cannot be very well constrained. In each case, we have therefore set N_H to the most accurate value measured

so far (i.e by ASCA/ROSAT/*Beppo-SAX*). In order to account for the uncertainties in the relative calibration of the PCA and HEXTE experiments, we have also left the relative normalization of the two spectra as a free parameter of the model used.

To investigate the systematics in the PCA data and to validate our analysis scheme, we have first analyzed a 15 kilo-second Crab observation (March 22, 1997). We have found that to get acceptable fits, it was necessary to add a systematic error to the data to reduce the effects of the imperfect knowledge of the instrument response near the K and L edges of xenon. These errors derived from looking at the residuals of the power law fit are 0.5% between 2.5 and 15 keV, 1% between 15 and 25 keV and 2.5% above. Fitting the Crab spectrum between 2.5 and 25 keV thus yields a $\chi^2_{\text{d.o.f}}$ of 1.0 (50 d.o.f.), a power law index of 2.18, and a normalization at 1 keV of 13.5 Photons $\text{cm}^{-2} \text{s}^{-1} \text{keV}^{-1}$ ($N_{\text{H}} = 3.3 \times 10^{21} \text{H atoms cm}^{-2}$ being frozen during the fit). The ratio between the data and the power law folded through the response matrix is shown in Fig. 8. A similar level of systematics has been used by several groups (e.g. Rothschild et al. 1999, Wilms et al. 1999, Bloser et al. 1999). Based on this, before the fitting, we have combined quadratically to the Poisson errors of our data, this level of systematics using the FTOOLS *grrpha* version 5.7.0. No systematic errors were added to the HEXTE data.

3.1. The RXTE observations

The RXTE observations are summarized in Fig. 2, 3, 4 and 5, for 1E1724–3045, GS1826–238, SLX1735–269, and KS1731–260. These figures represent the HEXTE background-subtracted light curve (top panel), the PCA 2-40 background-subtracted light curve (underneath), the PCA color-color diagram (soft color: 7-15 keV/2-7 keV, hard color 15-40 keV/7-15 keV (bottom left panel), and a PCA hardness intensity diagram (bottom right panel). For clarity and homogeneity, the data from orbits contaminated by bursts have been filtered out (only data recorded with the 5 PCA units ON are shown).

The observation of 1E1724–3045 started on November 4th, 1996 (T0=11h 54mn 39s), and was spread over more than 4 days. During the observation, an X-ray burst occurred on Nov. 8th at 05h 30mn 07s (UT). As said above for KS1731–260, a

few NSs exhibit nearly coherent pulsations during X-ray bursts. Sampling the burst profile each second, we have searched for such a coherent signal in both the *science event* and *burst catcher* mode data. No significant signals were detected between 200 and 1500 Hz. Data from the orbit when the burst occurred and the next one have been removed from the present analysis. The source did not display any significant variability over the observation. In addition, looking at the color-color diagram, one can see that it was observed in a single spectral state (see also, Olive et al. 1998). A single PCA spectrum averaged over the whole observation has thus been considered for the spectral analysis.

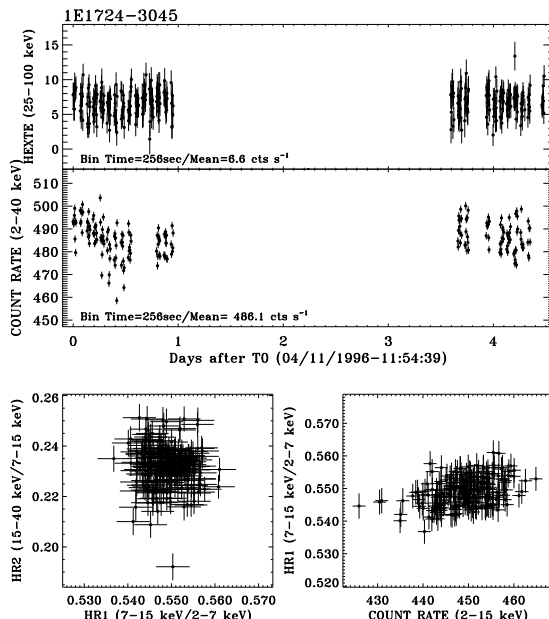


Fig. 2.— *Top* HEXTE 25-100 keV hard X-ray light curve with underneath the 2-40 keV PCA light curve of 1E1724–3045 over the 4.5 day span of our observation. *Bottom left* The color-color diagram (the soft color HR1 is the ratio 7-15 keV/2-7 keV and the hard color HR2 is 15-40 keV/7-15 keV) and *Bottom right* the hardness-intensity diagram for the soft color. Only PCA data recorded with the 5 PCA units ON are shown (this explains the first gap in the PCA light curve while HEXTE was recording data).

GS1826–238 was observed between November 5th and 6th, 1997 for about 50 msec also (T0=08h

22mn 39s, UT). There are two bursts in the middle of the observation. As for 1E1724–3045, no coherent pulsations were detected in those bursts. The time separation between the two bursts is ~ 5.6 hours, consistent with the 5.76 hours (1σ spread of 0.26 h) periodicity reported by Ubertini et al. (1999). In addition, from this periodicity, one expects a burst to have occurred ~ 1600 seconds before the beginning of our observation. The tail of this burst is clearly seen in the first orbit of data. Data from this orbit, as well as from those contaminated by the two bursts, have been removed from the present analysis. The spectral analysis of these bursts and their impact on the persistent emission will be reported elsewhere. As shown in Fig. 3 the source intensity varies by as much as $\sim 10\%$ in the 2-40 keV range, but the source did not display significant spectral variability. As for 1E1724–3045, a single PCA spectrum was then used in the spectral analysis. In the hard X-ray band, it is the brightest of the sources considered here (the count rate in HEXTE-Cluster A is 8.0 cts s^{-1} in the 25-100 keV range).

SLX1735–269 was observed in October 10th, 1997 (T0=04h 37mn 19s); its observation which was scheduled for 50 ksec ended 2.5 days later. The mean PCA count rate is 165.5 cts s^{-1} (2-40 keV), and this is the faintest of the four sources considered here. No X-ray bursts were observed. The source is clearly variable on minute time scales. However it is clear that these intensity variations are not accompanied by strong spectral changes, as the source remains in a limited region in the color-color diagram.

Finally, the observation of KS1731-260 started on October 28th, 1997 (T0=22h 20mn 15s, UT), lasted for about 50 ksec, and ended on October 30th. In the PCA, KS1731-260 has the largest count rate of the sources considered here. The so-called banana shape is clearly visible on the color-color and hardness intensity diagrams. It moves from the lower to the upper parts of the banana as the count rate increases (by up to $\sim 25\%$, 2-40 keV). Given the source variability, we have considered three PCA spectra in the spectral analysis; one for each day of the observation. It is detected by HEXTE only up to ~ 50 keV. No X-ray bursts were detected.

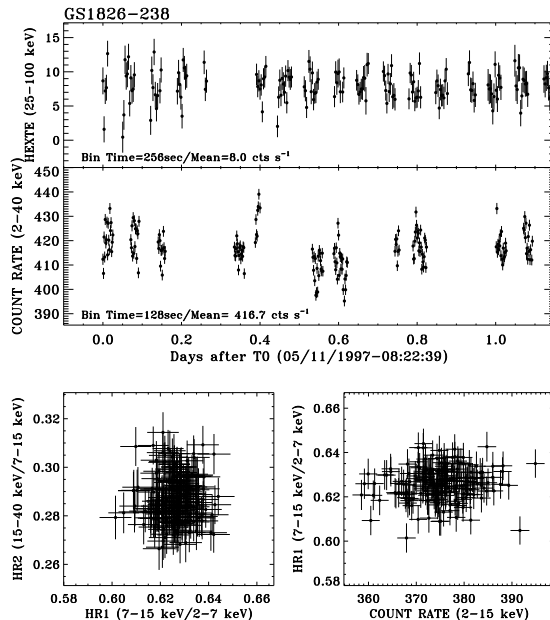


Fig. 3.— *Top* HEXTE 25-100 keV hard X-ray light curve with underneath the 2-40 keV PCA light curve of GS1826–238 over the 1.2 day span of our observation. *Bottom left* The color-color diagram (the soft color HR1 is the ratio 7-15 keV/2-7 keV and the hard color HR2 is 15-40 keV/7-15 keV) and *Bottom right* the hardness-intensity diagram for the soft color. The data contaminated by X-ray bursts have been removed. Only PCA data recorded with the 5 PCA units ON are shown.

3.2. Timing properties

The normalized Power Density Spectra (PDS) averaged over the whole observation of all four sources are shown in Fig. 6. The first three sources show noise up to ~ 200 Hz. The integrated power of these PDS is 29.1%, 26.1%, 27.6% in the 2-40 keV band (0.005-300 Hz). In addition, they also show a break in the PDS at low frequencies (typically around 0.1-0.2 Hz), and a QPO-like feature around 1 Hz. Although the complete analysis is still under way (for GS1826–238 and SLX1735–269), no strong HFQPOs were detected from any of these three systems. For 1E1724–3045, for which a sensitive search has already been conducted, an upper limit of 2.5% on the RMS of a 1000 Hz QPO has been derived (5-30 keV) (Barret et al. 1999b).

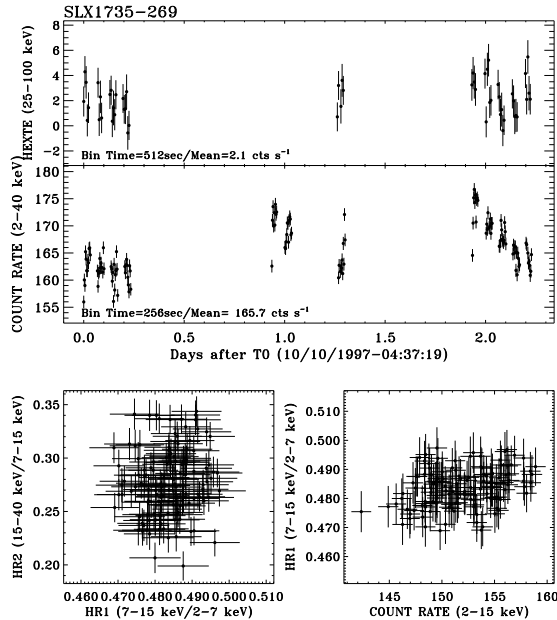


Fig. 4.— *Top* HEXTE 25-100 keV hard X-ray light curve with underneath the 2-40 keV PCA light curve of SLX1735–269 over the 2.5 day span of our observation. *Bottom left* The color-color diagram (the soft color HR1 is the ratio 7-15 keV/2-7 keV and the hard color HR2 is 15-40 keV/7-15 keV) and *Bottom right* the hardness-intensity diagram for the soft color. Only PCA data recorded with the 5 PCA units ON are shown.

The PDS shown in Fig. 6 for SLX1735–269 is very similar both in shape and normalization to the one reported by Wijnands & Van der Klis (1999a) from a short RXTE observation performed in February-May 1997. Although the source count rate did not change a lot during our observation (see Fig. 4), we have computed two PDS for segments of the observation associated with the highest and lowest count rates: 172 cts s^{-1} (156 cts s^{-1}) versus 162 cts s^{-1} (150 cts s^{-1}), 2-40 keV (2-16 keV), respectively. Fitting these two PDS with broken power laws yields a break frequency of 0.15 ± 0.1 Hz, and 0.08 ± 0.02 Hz respectively. Thus, within our limited range of intensity variations, the break frequency decreased with the count rate, a behaviour which is generally observed from atoll sources (Van der Klis, 1994). At lowest count rate, Wijnands & Van der Klis (1999a) reported the opposite behaviour between

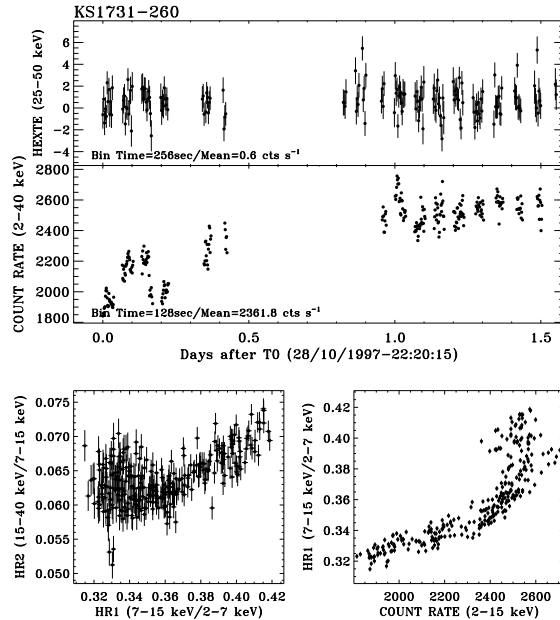


Fig. 5.— *Top* HEXTE 25-50 keV hard X-ray light curve with underneath the 2-40 keV PCA light curve of KS1731-260 over the 1.5 day span of our observation. *Bottom left* The color-color diagram (the soft color HR1 is the ratio 7-15 keV/2-7 keV and the hard color HR2 is 15-40 keV/7-15 keV) and *Bottom right* the hardness-intensity diagram for the soft color. Only PCA data recorded with the 5 PCA units ON are shown.

two segments of observations of count rates 141 and 113 cts s^{-1} (2-16 keV); ν_{Break} increased from 0.11 to 2.3 Hz. Therefore, this means that like in the case of the millisecond pulsar SAXJ1808.4-3658 (Wijnands & Van der Klis 1998), it appears that ν_{Break} correlates with the source count rate (the latter most likely tracking the mass accretion rate), down to a certain value, below which ν_{Break} and the source count rate anti-correlates. For both SLX1735–269 and the millisecond pulsar, this transition occurred at a luminosity of $\sim 2 - 4 \times 10^{36}$ ergs s^{-1} (3-25 keV).

KS1731-260 is characterized by weaker variability with an integrated power of $\sim 3.0\%$ (2-40 keV). Its PDS can be approximated by a PL of index $\alpha = 1.3$ on which a QPO centered at 7.6 ± 0.7 Hz is superposed (FWHM = 3.1 ± 2.0 Hz for a gaussian fit). This QPO is very similar to the so-called “Horizontal branch” QPO observed in Z sources.

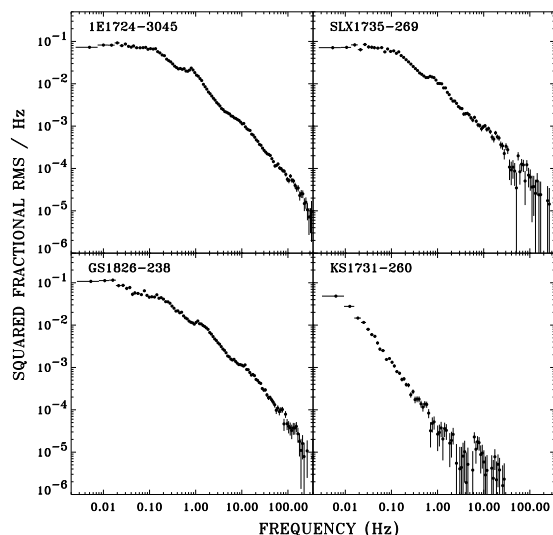


Fig. 6.— The power density spectra of all four sources averaged over the whole observations. 1E1724–3045, GS1826–238 and SLX1735–269 display high frequency noise extending up to 200–300 Hz with RMS amplitudes of 29.1%, 26.1%, 27.6% in the 2–40 keV band (0.005–300 Hz). KS1731–260 displays Very Low Frequency Noise with a RMS amplitude of $\sim 3.0\%$ (2–40 keV). These PDS are consistent with the first three sources being in the so-called island state (low state), and KS1731–260 being in the banana state (high state).

In addition, at higher frequencies, for the segment of the observation performed on October 28th (i.e. at the lowest count rate ~ 1050 cts s^{-1} , 5–30 keV), we have detected at the 4.7σ level a HFQPO centered at $\sim 1200 \pm 10$ Hz (FWHM= 45.0 ± 20 Hz, RMS= $2.5 \pm 0.4\%$)⁵. This is the highest HFQPO ever detected from KS1731–260. No HFQPOs were detected in the subsequent observations performed on October 29th (1285 cts s^{-1}) and 30th (1355 cts s^{-1}). We have derived an upper limit of $\sim 2\%$ on the RMS of any HFQPOs around 1000 Hz for the

⁵The 1200 Hz HFQPO observed is a lower limit of the Keplerian frequency at the innermost stable circular orbit (Kluźniak 1998, Miller et al. 1998). This translates into an upper limit on the mass of the NS: $M_{NS} \lesssim 1.83 \times (1 + 0.75j) M_{\odot}$, where $j = cJ/GM^2$ is a dimensionless stellar angular momentum, and $0.1 < j < 0.3$ for a NS spin frequency of ~ 260 Hz (Kluźniak 1998). This yields an upper limit of $2.25 M_{\odot}$ for the NS in KS1731–260.

October 29th and 30th observations, respectively. Our October 28th detection follows the correlation between the frequency of the HFQPO (ν_{HFQPO}) and the count rate, as well as the anticorrelation between ν_{HFQPO} and RMS presented in Wijnands & Van der Klis (1997).

3.3. Spectral fitting

Previous observations of similar NSs have shown that their broad band spectra can be generally fitted by the sum of two components (Mitsuda et al. 1984, White et al. 1988, Mitsuda et al. 1989). The first one is soft, contributes to the spectrum mainly below 10 keV, is modeled by a multi-color disk blackbody or a single temperature blackbody, and is interpreted as coming either from the accretion disk, or the NS surface, or an optically thick boundary layer (e.g. White et al. 1988, Mitsuda et al. 1984). The second one is harder and dominates the spectrum above 10 keV; it is often modeled by simple PLs (below 20 keV). However, when high energy coverage exists above 30 keV (e.g. with *Beppo-SAX* and RXTE), comptonization models provide more physical fits (e.g. Guainazzi et al. 1998, In’t Zand et al. 1999). The comptonization process is speculated to take place in a scattering corona located somewhere in the system; around the NS (e.g. optically thin boundary layer, spherical corona) or above the disk. In some cases, a relatively strong iron $K\alpha$ line (6.4 keV) is also observed above the continuum (e.g. White et al. 1986). In a few cases (e.g. 4U1608–522, Yoshida et al. 1993, SAXJ1808.4–3658, Gilfanov et al. 1998), such a line is accompanied by a broad absorption like feature, interpreted as partial absorption or reflection by a cold or weakly ionised medium of the intrinsic PL component. Hereafter we report on the results of the spectral analysis of our observations, placed in the framework of these previous results.

3.3.1. 1E1724–3045

Preliminary results of the analysis of the 1E1724–3045 spectral data can be found in Olive et al. (1999). In the present analysis, N_{H} has been set to the *ASCA/Beppo-SAX* value (i.e. 1.2×10^{22} H atoms cm^{-2}). Driven by the recent *Beppo-SAX* results, we have found that the broad band spectrum of 1E1724–3045 can be adequately described by the sum of two components; a soft

1E1724–3045

Parameter	C+BB+L	C+MCD+L
kT_E	$28.1^{+3.0}_{-3.0}$	$25.6^{+3.1}_{-2.0}$
kT_W	$1.1^{+0.1}_{-0.1}$	$1.6^{+0.2}_{-0.2}$
τ	$2.9^{+0.2}_{-0.2}$	$3.3^{+0.3}_{-0.3}$
kT_{BB}, kT_{in}	$0.6^{+0.1}_{-0.1}$	$1.2^{+0.1}_{-0.2}$
$R_{BB}, R_{in}\sqrt{\cos\theta}$	$10.1^{+2.3}_{-1.1}$	$2.8^{+0.2}_{-0.3}$
EqW	21^{+10}_{-9}	27^{+10}_{-10}
χ^2 (d.o.f)	79.9 (80)	85.7 (80)
F_{1-20} keV	1.52	1.58
F_{20-200} keV	0.90	0.91
f_{BB} (%)	14.4	27.2

Table 1: Best fit spectral results for 1E1724–3045. N_H has been set to 1.2×10^{22} H atoms cm^{-2} . The C+BB+L model is *Comptt*+Blackbody+a 6.4 keV narrow line ($\sigma_{Fe}=0.1$ keV), whereas C+MCD+L is *Comptt*+Multicolor Disk blackbody+a 6.4 keV narrow line. kT_E is the electron temperature in keV. kT_W is the temperature of the seed photons in the *Comptt* model (in keV). τ is the optical depth of the spherical scattering cloud. kT_{BB} is the temperature of the blackbody, kT_{in} is the inner disk color temperature derived from the MCD model. R_{BB} is the equivalent radius of the blackbody, whereas $R_{in}\sqrt{\cos\theta}$ is the projected inner disk radius (Mitsuda et al. 1984); they are both given in kilometers and scaled at the source distance (6.6 kpc). EqW is the equivalent width of the iron line in eV. The 1-20 keV flux (F_{1-20} keV) and hard X-ray 20-200 keV flux (F_{20-200} keV) are given in units of $\times 10^{-9}$ ergs $\text{s}^{-1}\text{cm}^{-2}$. f_{BB} is the contribution of soft component (BB or MCD) to the total luminosity computed in the 1-200 keV range. Errors in all the tables are quoted at the 90% confidence level ($\chi^2=\chi^2+2.7$).

and a hard Comptonized component well fitted by the *Comptt* model in XSPEC (Titarchuk 1994, Guainazzi et al. 1998, see also Barret et al. 1999). The soft component is well described by a BB ($\chi^2=88.1$, 81 d.o.f). A MCD could fit it as well, although the χ^2 is slightly larger ($\chi^2=92.3$, 81 d.o.f). For the Comptonizing cloud, we have derived an electron temperature (kT_E) of $\sim 27 - 30$ keV and an optical depth of $\sim 2.8 - 2.9$ and ~ 1.1 assuming that it has a spherical or disk-like geometry respectively. In both cases, a temperature of ~ 1.0 keV for the seed photons was derived. These parameters, which are listed in Table 1, are strikingly close to those found by Guainazzi et al. (1998), suggesting that in addition to its low variability in intensity (see Fig. 1), the source is also stable from the point of view of its energy spectrum. For the soft component, the best fit parameters are strikingly similar to those derived from the *Beppo-SAX* observations.

Independently of the model fitting the continuum, an excess around 6 keV seems to remain in the residuals. Assuming that it results from iron K fluorescence (6.4 keV), and that it is nar-

row ($\sigma_{Fe}=0.1$ keV), the *Comptt*+BB+Line model yields a χ^2 of 79.9 (80 d.o.f). The line equivalent width is 21 eV. In the remainder of this paper, we will assess the significance of additional components in the fitted model by means of the standard F-test. What we call the F-test probability will always refer to the probability of rejecting the correct hypothesis, which states that, with the additional component the fit is better. We define F_m as $(\chi_1^2 - \chi_2^2)/(\nu_1 - \nu_2)/(\chi_2^2/\nu_2)$ with $\chi_1^2 > \chi_2^2$ and $\nu_1 > \nu_2$ (where $\chi_{1,2}^2$ are the Chi-squared values of the two fits, with $\nu_{1,2}$ number of degrees of freedom, d.o.f.); F_m follows a Snedecor’s F distribution. In the present case, we have $F_m=8.2$, and $P(F > F_m)=0.005$, which means that the addition of the line to the *Comptt*+BB model is significant at the level of $\sim 99.5\%$. It is worth pointing out that the significance of any features in the spectrum depends strongly on the level of systematics added to the data, and that there are some uncertainties in the estimate of these systematics. To illustrate this, if instead of using 0.5% around 6 keV, one uses 1%, as for example in Rothschild et al. (1999), the significance of the line would drop

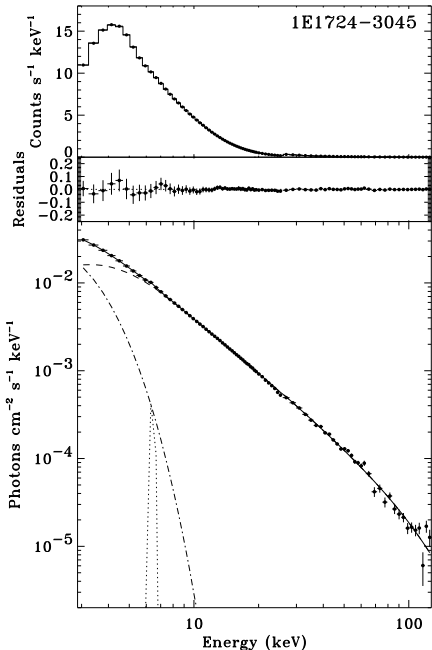


Fig. 7.— The data and folded model (top panel), the residuals (center panel) and the unfolded spectrum (bottom panel, Comptonized (*Comptt*) component is the dashed line, multi-color disk blackbody model is the dot-dashed line, the Gaussian line is the dotted line) of 1E1724–3045.

down to 85%, and hence the line detection would not be significant. Leaving the line energy and its width as free parameters does not improve the fit significantly. The presence of the line is also significant at the level of 98.5% for the *Comptt*+MCD model. However, since no such a line was found in ASCA and *Beppo-SAX* observations, we consider our detection very marginal. Fig. 7 shows the data and folded model (*Comptt*+BB+L), the residuals and the unfolded spectrum of 1E1724–3045.

For comparison with SIGMA data (35–200 keV), we have fitted the HEXTE data alone in the 25–150 keV range. Although the fit is not satisfactory due to the presence of a clear high energy cutoff (~ 70 keV), a PL fit yields a photon index of 2.7 ± 0.1 , to be compared with the time-averaged value observed by SIGMA (3.0 ± 0.3 , Goldwurm et al. 1993, 1994). Fitting the 2.5–25 keV PCA spectrum with a simple PL (note an acceptable fit) yields a photon index of ~ 2.0 . We therefore conclude that the steepness of the hard tail observed

by SIGMA was artificial, and due to the presence of a high energy cutoff around 60–70 keV. We have also fitted the continuum with the relativistic Comptonization model developed by Poutanen & Svensson (1996) (*CompPS* in XSPEC). For the Comptonized tail, this yields best fit parameters of 35 keV for kT_E and 2.1 for τ (spherical geometry assumed).

From this observation, we derive $L_{1-20 \text{ keV}} = 8.1 \times 10^{36}$ ergs s^{-1} , and $L_{20-200 \text{ keV}} = 4.8 \times 10^{36}$ ergs s^{-1} ($d=6.6$ kpc). $L_{1-20 \text{ keV}}$ is consistent with the time-averaged value derived from the ASM light curve.

3.3.2. GS1826–238

For GS1826–238, we have again set N_H to the value observed by ROSAT and *Beppo-SAX* (0.5×10^{22} H atoms cm^{-2}). To illustrate the complexity of the spectral shape, in Fig. 8, we show the ratio between the PCA data and a PL model folded through the PCA response matrix. There is a clear excess around 6.0 keV. First, of the single component models, the CPL is the one that provides the best fit. This yields a cutoff energy at ~ 95 keV and a photon index of 1.7 ($\chi^2=195.0$ for 87 d.o.f). A fit using a comptonization model (e.g. *Compst* in XSPEC) yields kT_E of 20 keV and an optical depth of 4.6. Adding a narrow 6.4 keV line ($\sigma_{Fe}=0.1$ keV) to account for the feature of Fig. 8 improves the fit ($\chi^2=149.4$ for 86 d.o.f) but still, the residuals show systematic deviations that indicate that this model is not the right description of our data.

Since a reflected component had been found in a combined analysis of the OSSE and GINGA data (Strickman et al. 1996), we have tested for the presence of such a component by adding an absorption edge at 7.1 keV. This leads to a significant decrease of χ^2 ($\chi^2=100.5$ for 85 d.o.f, $F_m=41.3$, $P(F > F_m) \gtrsim 7.9 \times 10^{-9}$). Thus we have substituted the CPL model by the XSPEC *Pexrav* model (Magdziarz and Zdziarski 1995), which is the sum of a CPL plus a Compton reflected component. The inclination angle to the source is unknown, but since GS1826–238 is not a dipper, we have assumed a standard value of $\theta = 60^\circ$, and we leave the reflection scaling factor as a free parameter (we assumed solar abundance for the reflecting material). This yields a reflection scaling factor of ~ 0.20 , and a narrow 6.4 keV line ($\sigma_{Fe}=0.1$ keV)

GS1826-238		
Parameter	CPL+L	CPL+R+L
Γ	$1.70^{+0.01}_{-0.02}$	$1.72^{+0.01}_{-0.01}$
E_{Cutoff}	$98.7^{+8.0}_{-7.0}$	$90.0^{+8.0}_{-7.0}$
f_{refl}	...	$0.15^{+0.03}_{-0.04}$
Line Energy	6.4 (fixed)	$6.1^{+0.3}_{-0.2}$
σ_{Fe}	0.1 (fixed)	$0.48^{+0.25}_{-0.23}$
EqW	36^{+8}_{-10}	50^{+17}_{-13}
χ^2 (d.o.f)	149.4 (86)	85.2 (83)
$F_{1-20 \text{ keV}}$	1.43	1.44
$F_{20-200 \text{ keV}}$	1.17	1.16

Table 2: Best fit spectral results for GS1826–238. N_{H} has been set to 0.5×10^{22} H atoms cm^{-2} . The CPL+L model is the sum of a Cutoff Power Law (Γ is the photon index, E_{Cutoff} is the cutoff energy in keV), plus a narrow 6.4 keV line ($\sigma_{\text{Fe}}=0.1$ keV). The CPL+L+R is the same but with the reflected component added (the CPL is substituted by the *Pexrav* model in XSPEC, Magdziarz and Zdziarski 1995), and the line energy and width (σ_{Fe}) left as free parameters of the fit. f_{refl} is the reflection scaling factor normalized to the CPL. It should be equal to 1 for an isotropic source above an infinite flat disk. Same units for $F_{1-20 \text{ keV}}$ and $F_{20-200 \text{ keV}}$ as in Table 1.

of EqW of 37 eV ($\chi^2=97.1$, 85 d.o.f.). The significance of the reflection component is very high ($F_m=45.4$, $P(F > F_m) \gtrsim 1.8 \times 10^{-9}$). Leaving the line energy and its width as free parameters of the model, we get $\chi^2=85.2$ (83 d.o.f.) with the line parameters: $\sigma_{\text{Fe}}=0.48$ keV, centroid energy at $6.1^{+0.3}_{-0.1}$ keV (90% confidence level, still consistent with a fluorescent iron $K\alpha$ line), and an EqW of 50 eV. This decrease of χ^2 is significant at the level of 99.7% ($F_m=6.0$, $P(F > F_m)=0.003$), we therefore conclude that this is the best fit to our data. As a further step, we have tried a reflection model including ionisation: *Pexriv* model in XSPEC (Magdziarz and Zdziarski 1995). This model fits the data as well as the *Pexrav* model ($\chi^2=95.5$, 84 d.o.f.), and yields a disk ionisation parameter consistent with 0. Therefore, with both models, our data are consistent with reflection from a cool neutral medium.

We have also reanalyzed the GINGA spectrum of GS1826–238 used in Strickman et al. (1996) and Zdziarski et al. (1999). The reflection component is highly significant, and consistent with coming also from a neutral medium also. A fit with a simple power law and a 6.4 keV narrow line yields $\chi^2=39.6$ for 31 d.o.f., while adding the reflection component yields $\chi^2=16.1$ for 29 d.o.f. ($F_m=21.2$, $P(F > F_m)=2.1 \times 10^{-6}$). The best fit parameters are $\Gamma=1.88 \pm 0.05$, and $f_{\text{refl}}=0.8 \pm 0.3$, and an

equivalent width for the iron line of 15 eV⁶.

There is no soft component in the source spectrum. With the *Pexrav* model, we have set a 90% confidence limit of about 1% on the fraction of 1-200 keV luminosity in the soft component modeled by a 1.5 keV BB component. The results of the best fit using the CPL+Line+Reflection model are given in Table 2. The data and folded model, the residuals and the unfolded spectrum of GS1826–238 are shown in Fig. 9.

For comparison with hard X-ray observations of similar systems, we have fitted the HEXTE spectrum with a PL. Although the fit is poor due to the presence of a clear cutoff in the spectrum, one gets a photon index of $\sim 2.3 \pm 0.2$, similar to the value derived for 1E1724–3045. Fitting the hard tail with the *CompPS* model yields $kT_{\text{E}}=41$ keV and $\tau = 1.9$.

For this observation, one derives $L_{1-20 \text{ keV}}=$

⁶The evidence for a reflection component is very strong in both the RXTE and GINGA data. It is therefore quite puzzling that no such component has been reported so far from the two *Beppo-SAX* observations performed, while GS1826–238 was at a similar intensity level (7.7×10^{-10} ergs $\text{s}^{-1}\text{cm}^{-2}$ for RXTE, as opposed to 5.5×10^{-10} ergs $\text{s}^{-1}\text{cm}^{-2}$ for *Beppo-SAX* (2-10 keV), Del Sordo et al. 1999, In't Zand et al. 1999). We are currently investigating this issue, searching for instrumental effects, sensitivity limits, and systematic errors in the fitting the continuum shape.

SLX1735–269

Parameter	CPL+MCD+L	CPL+MCD+R+L
Γ	$2.06^{+0.01}_{-0.01}$	$2.09^{+0.03}_{-0.04}$
kT_{in}	$0.53^{+0.06}_{-0.07}$	$0.44^{+0.10}_{-0.08}$
$R_{\text{in}}\sqrt{\cos\theta}$	$9.4^{+5.4}_{-2.9}$	$17.0^{+16.6}_{-9.1}$
f_{refl}	...	$0.28^{+0.09}_{-0.12}$
ξ_i	...	$70.1^{+740.2}_{-70.1}$
EqW	67^{+15}_{-157}	39^{+15}_{-14}
χ^2 (d.o.f)	45.2 (59)	28.4 (57)
$F_{1-20 \text{ keV}}$	0.72	0.75
$F_{20-200 \text{ keV}}$	0.39	0.30
$f_{\text{BB}}(\%)$	9.0	12.6

Table 3: Best fit spectral results for SLX1735–269. N_{H} has been set to 1.5×10^{22} H atoms cm^{-2} . The first model is the sum of CPL+MCD and a 6.4 keV narrow line. The best fit model is the sum of a CPL and its Compton reflected component (R) allowing for ionisation (*Pexriv* in XSPEC), a MCD, and a narrow 6.4 keV line (L) ($\sigma_{\text{Fe}}=0.1$ keV). The cutoff energy in *Pexriv* has been set to 200 keV and frozen during the fit. ξ_i is the ionisation parameter in *Pexriv*. The contribution for the Galactic diffuse component has been modeled by a Raymond-Smith model of 3.4 keV (normal abundance) and normalization factor of 1.5×10^{-2} in XSPEC units. See Table 1 for definition of f_{BB} and units of $F_{1-20 \text{ keV}}$ and $F_{20-200 \text{ keV}}$.

8.4×10^{36} ergs s^{-1} , and $L_{20-200 \text{ keV}} = 6.9 \times 10^{36}$ ergs s^{-1} ($d=7$ kpc). $L_{1-20 \text{ keV}}$ is very close to the time-averaged value derived from the ASM light curve.

3.3.3. SLX1735–269

A preliminary report of the spectral analysis of SLX1735–269 can be found in Skinner et al. (1999). As in the cases of GS1826–238 and 1E1724–3045, SLX1735–269 was observed in a hard state. However, it was a factor of two fainter than the other two sources, so that the statistical quality of the HEXTE spectrum is not as good. For that reason, we considered the HEXTE data only up to 50 keV. In our fits we fix N_{H} at 1.5×10^{22} H atoms cm^{-2} , found in David et al. (1997), as the ASCA data are more sensitive to this parameter. We have first fitted the PCA+HEXTE spectrum of SLX1735–269 with a simple PL. The fit is not good ($\chi^2_{\text{d.o.f}} \gtrsim 6.5$) but shows clear evidence for a broad feature around 6.4 keV (see Fig. 8). As no iron line was seen in the ASCA data, and because of the relative faintness of the source, we have first considered the possibility that the line might not be from the source but might represent the flux within the PCA 1° field of view from the galactic bulge diffuse emis-

sion. We have therefore included in our model a contribution from the spectrum given by Valinia & Marshall (1998) for their “Region 2” which includes this part of the sky. Refitting the data with this component affects the shape of the residuals at low energies ($\lesssim 5$ keV); they now clearly show the presence of a soft component and reveal that the broad feature between 6–7 keV cannot all be accounted for by the diffuse emission, meaning that there remains a need for a significant contribution from the source to the line. Such a line was also needed in the data analyzed by Wijnands & Van der Klis (1999). The soft component was fitted with a MCD (although the BB model fits the data equally well), whereas the line contribution from SLX1735–269 was modeled by a gaussian centered at 6.4 keV. This leads to a χ^2 of 45.2⁷ (59 d.o.f), and thus the addition of the line and soft com-

⁷For SLX1735–269, the χ^2 associated with the best fits are lower than 1 (see Table 3). This makes naturally questionable the results of our F-test. Similarly, the errors computed on the best fit parameters should not be considered as true 90% uncertainties (these errors are computed under the assumption that the errors on the data are Poissonian). The low χ^2 indicates certainly that for SLX1735–269, which is the faintest of the 4 sources, the systematics assumed are too large. However, for consistency in the analysis, we have chosen to set them to the values used for the other sources.

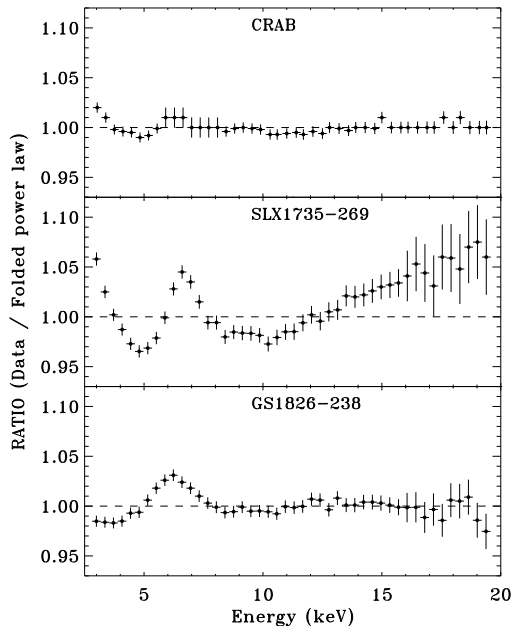


Fig. 8.— The ratio between the data and a folded power law model for the Crab, SLX1735–269 and GS1826–238. The response matrix used in the Crab analysis has been obtained using the same procedure as for the other sources. For GS1826–238 and SLX1735–269, this plot indicates the presence of a strong feature around 6–7 keV.

ponent is statistically significant based on our F-test. The EqW found (67 eV if the line is narrow, $\sigma_{\text{Fe}}=0.1$ keV) is well below the upper limits of 150 eV ($\sigma_{\text{Fe}}=0.1$ keV) derived by David et al. (1997) using ASCA SIS data.

However, by looking at the residuals above ~ 7 keV the data show systematic deviations with an edge-like shape. An edge around these energies is suggestive of the presence of a reflection component. We have therefore first substituted the PL model with the *Pexrav* model in XSPEC (assuming no energy cutoff in the model, and a 6.4 keV line with a $\sigma_{\text{Fe}}=0.1$ keV, an inclination angle of 60°). This leads to $\chi^2=31.4$ (58 d.o.f.), indicating that the presence of a reflected component is significant at a level greater than 99.99% ($F_m=23.1$, $P(F > F_m)=1.1 \cdot 10^{-5}$). The solid angle inferred is ~ 0.26 and the line EqW is 47 eV. Whether or not the reflector is ionised has been tested by us-

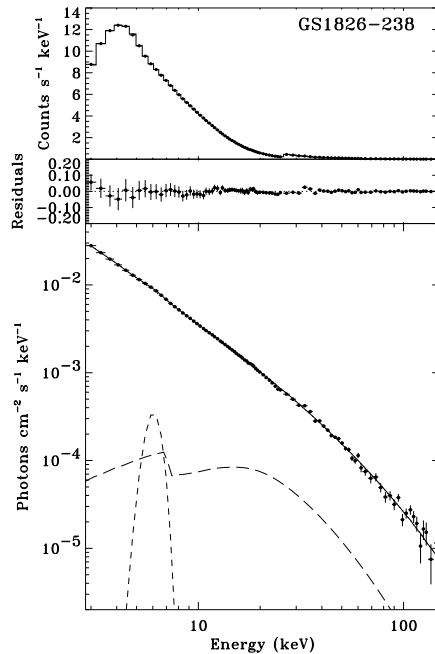


Fig. 9.— The data and folded model (top panel), the residuals (center panel) and the unfolded spectrum (bottom panel) of GS1826–238. The iron line at 6.4 keV is represented by the dashed line, the reflection component by the long dashed line.

ing the *Pexriv* model. The statistical quality of the data does not allow us to determine the line energy simultaneously with the Compton reflected component. We have assumed the line at 6.5 keV (expected from a moderately ionised medium). This yields a $\chi^2=28.4$ (57 d.o.f.), an ionisation parameter, albeit poorly constrained, of $\xi_i \sim 70^{+740}_{-70}$, a solid angle of ~ 0.28 and a line EqW of 39 eV (see Table 3). The improvement of χ^2 from the *Pexrav* to the *Pexriv* model is significant at the level of 98.3% ($F_m=8.8$, $P(F > F_m)=4 \times 10^{-3}$). It is worth pointing out that leaving out the line at 6.4 keV increases the significance of the ionisation of the reflector, but then the model becomes unrealistic, as the line is not expected to be at 6.4 keV for the ionisation parameters derived from the fit ($\xi_i \gtrsim 70$). To conclude, one can say that our data for SLX1735–269 are consistent with reflection from a neutral or moderately ionised medium.

In the absence of any cutoffs in the useful energy range of the present measurements, Comptonization models cannot really be used. We note

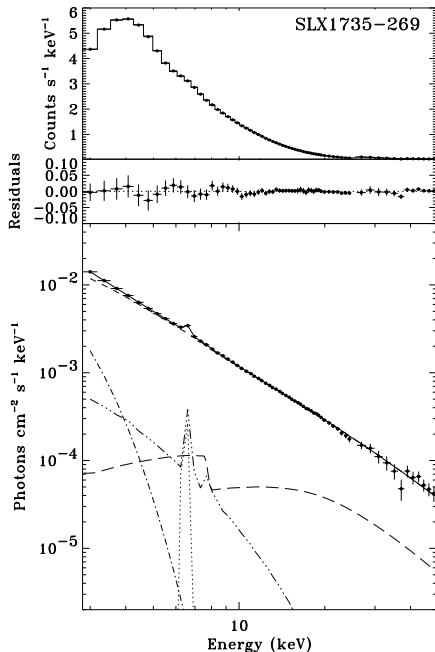


Fig. 10.— The data and folded model (top panel), the residuals (center panel) and the unfolded spectrum (bottom panel) of SLX1735–269. The power law component is represented by the dashed line, the multi-color disk blackbody model by the dot-dashed line, the iron 6.4 keV line by the dotted line and the reflection component by the long-dashed line. The Raymond-Smith thermal spectrum corresponding to the galactic diffuse emission around SLX1735–269 is also indicated as a dot-dot-dot dashed line.

however that a Comptonization model for which the electron temperature would be ~ 30 keV (as seen in 1E1724–3045) could fit the continuum as well as the PL. This would yield an optical depth of ~ 3 for the scattering cloud. Similar results were obtained by combining simultaneous ASCA and SIGMA data (Goldwurm et al. 1995). The best fit parameters are listed in Table 3 while the data and folded model, the residuals and the unfolded spectrum are shown in Fig. 10.

For this observation, we derive $L_{1-20 \text{ keV}} = 6.0 \times 10^{36}$ ergs s^{-1} , and $L_{20-200 \text{ keV}} = 3.5 \times 10^{36}$ ergs s^{-1} ($d=8.5$ kpc). $L_{1-20 \text{ keV}}$ is about a factor of two lower than the time-averaged value derived from the ASM light curve.

3.3.4. KS1731-260

KS1731-260 was observed in a high state, and its spectrum is clearly much softer than the other three sources examined before. We have assumed the N_H measured by ROSAT and ASCA (i.e. 1.2×10^{22} H atoms cm^{-2}). As the source intensity increased smoothly during our 3-day observation, and its intensity variations are accompanied with spectral variations (see Fig. 5), as said above we have made a PCA spectrum for each of the three days. These PCA spectra were fitted simultaneously with a single HEXTE spectrum averaged over the whole observation to increase the statistics at high energies.

We first analyzed the October 28th spectrum. As there is a clear cutoff in the spectrum around 10 keV, we have first fitted the continuum with a simple comptonization model (*Compst*). This model alone is clearly rejected ($\chi^2 \gtrsim 977$ for 55 d.o.f). This is mainly due to the presence of a broad feature again centered around 6.4 keV. We have therefore added an iron K fluorescence line (6.4 keV) and fitted its width and intensity. This improves the fit significantly ($\chi^2 = 156.2$ for 53 d.o.f). However, looking at the residuals indicates that the low energy part of the spectrum is not well accounted for. As in similar systems, a soft component (either a blackbody or a disk blackbody) is usually observed (e.g. White et al. 1988), we have included such a component in the fit. This again improves the fit ($\chi^2 = 48.6$ for 51 d.o.f., $F_m = 56.5$, $P(F > F_m) = 1.2 \times 10^{-13}$) for addition of the BB model. We have tried to fit the “hard” component with a MCD model (Mitsuda et al. 1984), instead of using *Compst*, but the fit is rejected, as the reduced χ^2 exceeds 4. On the other hand, the soft component could equally well be fitted with a MCD. For both models, the equivalent radius of the BB and the projected inner disk radius of the MCD are small; $R_{BB} \lesssim 5$ km and $R_{in} \sqrt{\cos \theta} \lesssim 4$ km respectively, smaller than the NS radius, or the expected inner disk radius around a NS (especially if the NS is as massive as $2M_\odot$, see above). This does not mean however that the models can be ruled out, because for instance only a small fraction of the NS surface could be involved in the emission, or alternatively some fraction of the disk flux could be intercepted and scattered up in a corona.

KS1731-260

	28/10		29/10		30/10	
	C+L+MCD	C+L+BB	C+L+MCD	C+L+BB	C+L+MCD	C+L+BB
kT_E	$2.8^{+0.2}_{-0.1}$	$2.8^{+0.2}_{-0.1}$	$2.7^{+0.1}_{-0.1}$	$2.6^{+0.1}_{-0.1}$	$2.6^{+0.1}_{-0.1}$	$2.6^{+0.1}_{-0.1}$
τ	$10.6^{+0.4}_{-0.6}$	$10.4^{+0.2}_{-0.3}$	$12.1^{+0.5}_{-0.7}$	$11.8^{+0.2}_{-0.3}$	$13.3^{+0.5}_{-0.6}$	$12.6^{+0.5}_{-0.2}$
σ_{Fe}	$0.9^{+0.1}_{-0.2}$	$0.9^{+0.1}_{-0.2}$	$0.8^{+0.2}_{-0.1}$	$0.8^{+0.2}_{-0.1}$	$0.8^{+0.2}_{-0.2}$	$0.7^{+0.3}_{-0.2}$
kT_{in} or kT_{BB}	$1.8^{+0.2}_{-0.2}$	$1.3^{+0.1}_{-0.1}$	$1.7^{+0.2}_{-0.2}$	$1.2^{+0.1}_{-0.1}$	$1.3^{+0.2}_{-0.1}$	$1.0^{+0.2}_{-0.1}$
$R_{in}\sqrt{\cos\theta}$ or R_{BB}	$2.2^{+0.5}_{-0.3}$	$3.8^{+0.5}_{-0.4}$	$2.5^{+0.8}_{-0.5}$	$3.8^{+1.2}_{-0.2}$	$3.9^{+1.9}_{-1.5}$	$4.7^{+4.4}_{-1.4}$
EqW	154^{+29}_{-26}	136^{+32}_{-29}	118^{+30}_{-25}	106^{+32}_{-27}	94^{+35}_{-26}	86^{+37}_{-28}
χ^2 (d.o.f)	50.6 (51)	48.6 (51)	45.7 (51)	43.9 (51)	51.4 (51)	51.2 (51)
F_{1-20} keV	8.4	8.7	9.4	9.6	9.5	9.6
F_{20-200} keV	0.07	0.07	0.08	0.08	0.09	0.09
f_{BB} (%)	13.5	6.3	13.0	5.9	9.8	3.2

Table 4: Best fit spectral results for KS1731-260 for three segments of the observation (Oct 28th, 29th, 30th). N_H has been set to 1.3×10^{22} H atoms cm^{-2} . The best fit model is the sum of a *Compst* model (C), a MCD or a BB, and a 6.4 keV gaussian line of fitted width (σ_{Fe}). $R_{in}\sqrt{\cos\theta}$ and R_{BB} are scaled at 8.8 kpc. See Table 1 for definition of f_{BB} and units of F_{1-20} keV and F_{20-200} keV.

We have also tried the *Comptt* model for the Comptonized component. However, the temperature for the seed photons (kT_W) is typically 0.2-0.3 keV, and is therefore unreliable since the peak of the Wien law, at $3kT_W$, is also below 2.5 keV (the peak is needed for kT_W to be determined reliably). For the comptonizing cloud, kT_E are consistent between *Comptt* and *Compst*, whereas τ is a factor of ~ 2 lower for *Comptt* than for *Compst* (spherical geometry assumed).

The broadening of the line (due to Comptonization?) is significant. Assuming the line is narrow ($\sigma_{Fe}=0.1$ keV), we obtain a larger χ^2 (87.1 for 52 d.o.f). The hypothesis that the line is narrow is therefore rejected at more than 99.99% confidence level ($F_m=40.4$, $P(F > F_m)=5.6 \times 10^{-8}$). If one leaves the energy of the line as a free parameter, its value tends to move towards lower energies (~ 6.2 keV, $\chi^2=46.1$ for 50 d.o.f). However, this shift of the line energy is not significant ($F_m=2.1$, $P(F > F_m)=0.14$).

If an iron line of EqW of $\sim 100 - 150$ eV is present, one might expect to detect also a Compton reflection component. First adding an edge at 7.1 keV (cool iron) never improved the fit significantly (significance always lower than 95%, the line energy and width were kept fixed). Similarly, we tried to fit the data with the *Pexrav* model, as a substitute to the *Compst* model. This never im-

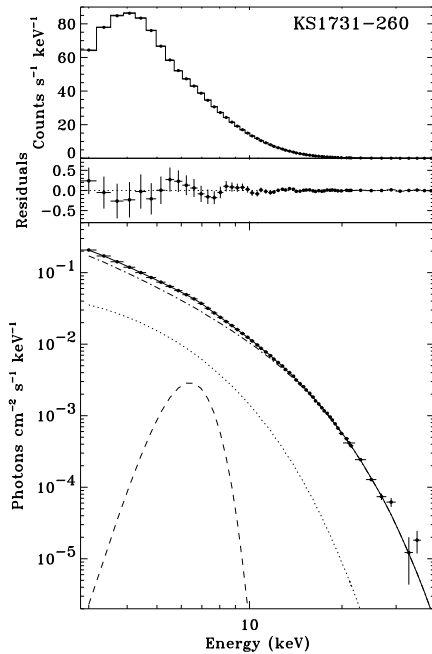


Fig. 11.— The data and folded model (top panel), the residuals (center panel) and the unfolded spectrum (bottom panel) of KS1731-260 for the October 28th observation. The contribution from the *Compst* component is shown by a dot-dashed line, the blackbody is the dotted line, whereas the broad iron line is shown with a dashed line.

proved the fit either. The non detection of such a component might be simply related to the curve shape of the spectrum (in particular the continuum is not a CPL as assumed in *Pexrav*); reflection is easier to observe when the continuum is PL-like (Note that if there is indeed a reflection component; this will affect the fitted parameters for the continuum and hence the strength of the iron line).

The same model is also the best fit of the October 29th and 30th spectra. In Table 4, we list the best fit parameters for the *Compst*+BB+Line and *Compst*+MCD+Line models. The data and folded model, the residuals and unfolded spectrum KS1731-260 for October 28th are shown in Fig. 11.

For KS1731-260, $L_{1-20 \text{ keV}}$ was $\sim 8.0 \times 10^{37} \text{ ergs s}^{-1}$ at the beginning of the observation and reached $\sim 9.1 \times 10^{37} \text{ ergs s}^{-1}$ at the end ($d=8.8 \text{ kpc}$). Such X-ray luminosity is slightly larger than the time averaged ASM value. Throughout the observation, $L_{20-200 \text{ keV}}$ contributed just at the level of $\sim 1\%$ to the 1-200 keV luminosity of the source.

4. Discussion

We have here reported RXTE PCA+HEXTE timing and spectral observations of four type I X-ray bursters (hence NSs). In the remainder, first we discuss their timing properties, then their broad band spectral properties, and finally address issues concerning possible differences between BHs and NSs.

4.1. Timing properties

1E1724-3045, SLX1735-269 and GS1826-238 were in a so-called low state (LS) whereas KS1731-260 was in a high state (HS). The LS sources all have very similar PDS, characterized by High Frequency Noise (HFN, or flat top noise, Van der Klis 1994) with large RMS amplitudes (30%, 2-40 keV). 1E1724-3045 and SLX1735-269 are characterized by the presence of a $\sim 1 \text{ Hz}$ QPO, and a break (at ν_{Break}) at 0.1-0.2 Hz. For GS1826-238, depending on the modeling of the PDS, $\nu_{\text{Break}} \sim 0.02 \text{ Hz}$ or $\sim 0.2 \text{ Hz}$, and $\nu_{\text{QPO}} \sim 0.2$ or $\sim 1.0 \text{ Hz}$. KS1731-260 has a very different PDS, displaying both Very Low Frequency Noise (VLFN) and a QPO at $\sim 7.6 \text{ Hz}$. These properties are all consistent with those of “atoll” sources at vary-

ing luminosities; the 3 LS sources would be in the “island” state, whereas KS1731-260 would be in the “banana” state, according to the terminology defined by Hasinger & Van der Klis (1989).

4.1.1. Origin of the high frequency noise?

The high frequency noise is seen only in sources displaying significant hard X-ray emission (all sources except KS1731-260), and hence must be related to the existence of a hot scattering cloud. This noise in the PDS is very similar in shape and normalization to that seen from LS BHs, strongly suggesting that the same physical mechanism is responsible for the spectrum and variability in these systems. Since the spectral shape strongly suggests thermal Compton up scattering, then the variability must have something to do with varying either the seed photons, or optical depth, or the dissipation in the hot region.

The overall PDS shape can be described by a superposition of randomly occurring flares (or “shots”), generally with some distribution of event durations. Such “shot noise” models can give a good description of the PDS (Lochner et al. 1991 and references therein, Miyamoto et al. 1992, Nowak et al. 1999, Olive et al. 1998), but are only a phenomenological, rather than a physical, description of the variability. To get a physical description requires associating the “shots” to changes in the comptonizing cloud.

The simplest variability to envisage is a change of the soft photon input. Thermal comptonization involves multiple scattering of these seed photons on the hot electrons, so the spectrum at lower energies responds first, followed after several scattering timescales by the higher energy spectrum. Such models predict that there should be time lags between the hard and soft energy bands, but that these lags (which are simply a measure of the size of the scattering cloud) should be constant irrespective of whether the input variability was a short flare or a longer event. This directly conflicts with the observed lags in the BHCs (Miyamoto et al. 1988) and the NSs (Ford et al 1999), which clearly show longer lags for longer timescale variability (Miyamoto et al. 1991).

A satisfactory explanation of the long timescale lags is difficult. If the variability arises from varying the seed photons then the length of the lag

directly implies that the region is large. This led Kazanas, Hua and Titarchuk (1997) to develop the “Extended Atmosphere Comptonization Model” (see also Hua, Kazanas & Cui 1999). This assumes a source of white noise at the center of the scattering cloud which has a density profile $n(r) \propto 1/r$ out to radii of a few light seconds. Their inhomogeneous density distribution appears to match the observed time lags, and source spectra, but the physical situation is very hard to envisage. The majority of the gravitational potential energy is close to the compact object, so how can this power a hot corona whose size is many orders of magnitude larger? Another weakness of that model, is that it produces different PDS at different energies, contrary to what is observed (e.g. Nowak et al., 1999, Olive et al. 1998).

An alternative model which can fit the PDS and time lags but with a small source size has been developed by Poutanen & Fabian (1999). Here they associate the “shots” with magnetic flares above a cold accretion disk, and use the spectral evolution of the flares to produce the long lags. The flare begins with electrons being heated but the background disk seed photon density is high, so the early time flare spectrum is soft. As the heating progresses, the energy dissipated in the flare dominates that of the disk, so the spectrum becomes hard. The drawback with such models is that they rely on details of the magnetic dissipation, which are not well known. Nonetheless, it is encouraging that at least under some circumstances the lags and PDS can be matched by the envisaged small source.

4.1.2. *Origin of low frequency QPOs?*

The origin of the ~ 1 Hz QPO (at ν_{QPO}) in the LS sources, once suspected to be a BH signature, is also unknown, and is not accounted for by the above models. Chen & Taam (1994) have proposed that they might arise from disk luminosity oscillations resulting from thermal viscous instabilities developing within the inner disk region. Vikhlinin et al. (1994) have also suggested that they could result from a weak interaction between the “shots” when the instability is triggered in a region of stable energy supply. To keep the energy released constant on large timescales, the appearance of a strong shot should affect the amplitude and the probability of occurrence of sub-

sequent “shots”. Recently, developing a model specific for NSs (i.e. not accounting for the similarities between BHs and NSs), Titarchuk & Osherovich (1999) have associated the QPOs with radial oscillations in a boundary layer.

It has been shown that in many sources there exists a strong correlation between ν_{Break} and ν_{QPO} (Wijnands & Van der Klis 1999b). Our three LS sources follow this correlation (Olive & Barret 1999). This correlation suggests that the longest fluctuations (scaling as ν_{Break}^{-1}) and the QPOs are related to the same unknown physical mechanism or are produced in regions interacting with each other. Since the same correlation is observed among BHs and Z-sources, this mechanism cannot be related to the presence of a hard surface or even a small magnetosphere. In addition, in several systems (e.g. 4U1608-52, Yoshida et al. 1993, see however above for SLX1735-269), a strict correlation between ν_{Break} and the inferred mass accretion rate has been observed. For BHs, Esin et al. (1998) have speculated that the rapid variability that is associated with the hard X-ray emission could originate from an ADAF, with the variability timescales determined by the viscous or dynamical timescales in the ADAF. They have further proposed that the 1-10 Hz QPOs could result from the interactions at the boundary (the so-called transition radius in ADAF terminology) between the ADAF and the outer cool accretion disk, in which case the ν_{QPO} would be some multiples of the Keplerian frequency at the transition radius. Hence, a shrinking of the inner disk radius (possibly due to an increase in the mass accretion rate through the disk) should result in an increase of the QPO frequency. The correlation between the position of the inner disk radius inferred from the kilo-Hz QPO frequency and ν_{QPO} , observed for instance in 4U1728-34 (Ford et al. 1998), is consistent with the above picture. Furthermore, if ν_{Break} is somehow related to the size of the ADAF, the observed correlation between ν_{Break} and ν_{QPO} would imply that the ADAF contracts when the accretion rate increases (possibly due to an increase of cooling flux from the disk).

4.1.3. *Spectral states and high frequency QPOs*

Finally, in the three sources displaying high frequency noise and a hard X-ray tail, no HFQPOs (above 300 Hz) are detected (e.g. 1E1724-

3045, Barret et al. 1999b). More generally, it seems that no HFQPOs are seen when ν_{Break} is low ($\lesssim 6 - 7$ Hz; e.g. 4U1705-44, Ford et al. 1998). The lack of HFQPOs might therefore be related to the presence of a hot scattering corona. Smearing of the HFQPO signal in such a corona is a possible mechanism, which is however invoked at higher accretion rates (i.e. for larger optical depth $\tau \gtrsim 5$, cooler corona, Brainerd & Lamb, 1987). This might indeed explain the disappearance of the HFQPOs after it has reached saturation (i.e. when the inner disk is at the last stable orbit, e.g. 4U1820-30, Bloser et al. 1999), or more generally when the source enters the upper branch of the “banana” state (Miller et al. 1998). The anticorrelation between the QPO amplitude and the QPO frequency observed in KS1731-260 (see above) is consistent with this picture (note that there is a weak indication that the optical depth derived from the spectral fitting increases when the source luminosity increases, see Table 4). For the LS sources, from the spectral analysis, we have derived an optical depth of a few for the Comptonizing cloud. Could that cloud, through smearing, account for the lack of HFQPOs? Using our upper limit, one can set a lower limit on the size of the scattering region. If the radiation is scattered, the RMS amplitude at infinity (A_∞) of a luminosity oscillation with frequency ν and amplitude A_0 at the center of a spherical region of radius R_C and optical depth τ is $A_\infty \approx (2^{\frac{3}{2}} x e^{-x} + e^{-\tau}) A_0$, where $x = \sqrt{3\pi\nu R_C \tau / c}$ (ν is the frequency of the oscillation, Kylafis & Phinney, 1989; Miller et al., 1998). For a beaming oscillation, the attenuation is stronger (due to the fact that the scattering process tends to isotropize the photon distribution), and a factor $2/(1 + \tau)$ has to be multiplied to the first term of the previous equation (Kylafis & Phinney, 1989). Let us first consider $\nu = 300$ Hz, from the previous expression, taking $A_\infty = 2.5\%$ (our upper limit), assuming $R_C = 200$ km, one can set an upper limit ~ 4 and $\sim 6\%$ on A_0 for a luminosity and beaming oscillations, respectively. For a signal at 1000 Hz, these upper limits become 12% and 20% respectively. Alternatively, if we assume $A_0 = 10\%$, for the signal to be attenuated down to our upper limit, the size of the corona has to be larger than 100 km and 130 km for a beaming and luminosity 1000 Hz oscillation. Clearly, this indicates that with the low optical depth derived

for the comptonizing cloud, and for any plausible sizes of such a cloud, the attenuation is not very strong, and if signal there is, it has to be intrinsically weak.

Another possibility which may explain the lack of HFQPOs in LS sources might be related to the position of the inner disk radius. Obviously, if the HFQPOs are generated in the disk, and if the inner edge of the disk lies at large radius (see below), no signals at such high frequencies should be seen. In that respect, it is worth pointing out that the bump (around 10 Hz) in the PDS of 1E1724–3045 (Fig.6) was interpreted by Psaltis et al. (1999) as a low frequency kilo-Hz QPO (the same bump is seen in GS1826–238 and SLX1735–269). Their conclusion was derived from the fact that the 0.8 Hz QPO and the bump at 10 Hz fitted in the global correlation observed over several frequency decades between ν_{QPO} and the frequency of the lower kilo-Hz QPOs (Psaltis et al. 1999).

4.2. Spectral properties

To first order, the broad band LS spectra of NSs can be approximated with a PL followed by an exponential cutoff at 50-80 keV. There is also a weak soft component in 2 of the 3 LS sources, with temperature of $\sim 0.5 - 1$ keV contributing less than $\sim 30\%$ of the total luminosity. The latter quantities, when derived from the fit of PCA data are subject to uncertainties because the fit starts at 2.5 keV, because they depend on the N_{H} values assumed, and because there are some calibrations uncertainties of the PCA at low energies ($E \lesssim 5$ keV). However, as for example in the case of 1E1724–3045, the values derived from our spectral fitting are consistent with the ones obtained from observations that are more sensitive to such a soft component (e.g. by *BeppoSAX* or *ASCA*, Guainazzi et al. 1998, Barret et al., 1999a). Thermal Comptonization of these soft photons by hot electrons then appears to be the most plausible emission mechanism for these systems, and for a spherical scattering cloud, the derived optical depths and electron temperatures are in the ranges of $2 \lesssim \tau \lesssim 4$ and $15 \lesssim kT_{\text{E}} \lesssim 30$ keV. Thermal Comptonization also dominates the spectral formation in KS1731-260, but with a significantly lower kT_{E} (~ 3 keV) and larger τ (~ 10). The main difference between a source in the HS and a source in the LS is best illustrated in Fig.

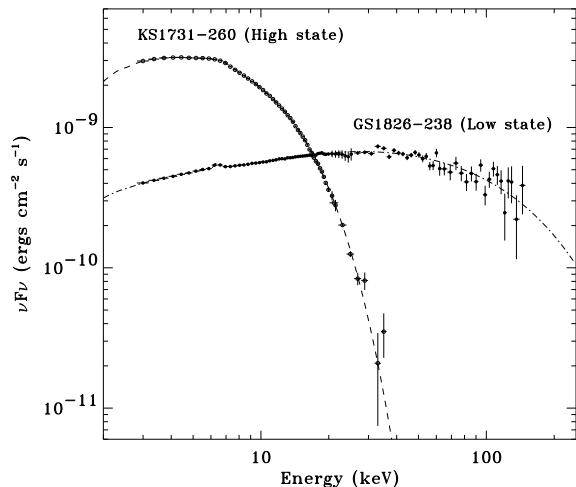


Fig. 12.— A $\nu F\nu$ plot of the spectra of KS1731-260 (high state) and GS1826-238 (low state). For KS1731-260, the bulk of the energy is radiated below ~ 7 keV. For GS1826-238, on the other hand, its spectrum is relatively flat, peaks around 40 keV and drops rapidly above 100 keV. No scaling for the different source distances has been performed.

12, where a $\nu F\nu$ plot of the PCA/HEXTE spectra of KS1731-260 and GS1826-238 are shown. Clearly for KS1731-260, the bulk of the energy is radiated below ~ 10 keV, whereas for GS1826-238 the energy spectrum is flatter and a large fraction ($\sim 50\%$) of the energy is radiated in the hard X-ray band.

4.2.1. Iron line emission and reflection in NS LMXBs

There is strong evidence for iron line emission in 2 out of the 3 LS sources examined here (the evidence is weaker for 1E1724-3045). The derived line energy is consistent with 6.4–6.5 keV, i.e. fluorescence from neutral/moderately ionised iron. There are three possible sites for line emission in LMXBs, the NS surface itself, the accretion disk, and accretion disk coronal wind. Any line from the NS would be strongly redshifted, down to ~ 5 keV, while the accretion disk corona should be strongly ionised, producing iron lines at 6.7 and 7.0 keV. Thus, the most likely origin for the observed 6.4 keV line is irradiation of the accretion disk by the X-ray source. If so, then it should be accompanied by a Compton reflected spectrum. We sig-

nificantly detect a neutral reflected continuum in GS1826-238, and a neutral/moderately ionised reflected continuum in SLX1735-269.

The reflection albedo, the ratio between the reflected and incident luminosities, is then an *observationally* determined quantity from our data. The reflection probability is determined by the relative importance of electron scattering and photo-electric absorption. At low energies the X-ray photons tend to be photo-electrically absorbed rather than scattered, so the reflection probability is low, while at higher energies the opposite is true. The photo-electric absorption probabilities are determined by both the element abundances (more heavy elements mean more hard X-ray opacity and so less reflection) and ionisation state (high ionisation states mean less bound electrons, so less opacity and more reflection). Beyond 10-20 keV, the photo-electric opacities become negligible in comparison to the electron scattering probability, but at these energies the electron scattering is not elastic. The incoming photon can lose much of its energy to the electron as it scatters, leading to a marked decrease in the reflected probability above 50–100 keV. Thus, even high energy photons can dump most of their energy in the disk. For hard spectra, such as those seen in GS1826-238, the *maximum* albedo, even with complete ionisation of the disk is $a_x \sim 0.75$, while the *observed* albedo is much less, at ~ 0.25 , because the ionisation state of the reflecting material is low/moderate, so most of the low energy incident flux is photo-electrically absorbed rather than reflected. For the HS spectra, such as KS1731-260, the reflection albedo can be much higher if the disk is completely ionised, since the spectrum is much softer. This is important because the disk heating and hence optical/UV reprocessed X-ray flux is determined by the non reflected flux, $(1 - a_x)$. Various attempts to derive the albedo from the optical reprocessed flux (e.g. de De Jong, van Paradijs & Augusteijn 1996) give $a_x \sim 0.9$. This is not in conflict with our values since most of the LMXBs considered were in the high state, where much more of the spectrum can be reflected. However, we caution that the optical determinations assume that the disk shape is that given by Vrtilik et al. (1990), with height $\propto r^{9/7}$. This was derived assuming that the disk is isothermal with height (central temperature equal to surface temperature), which

is incorrect (e.g. Dubus et al. 1999).

While the fraction of incident to reflected flux depends on the X-ray albedo (which in turn is given by the elemental abundances and ionisation state of the reflector and the spectral shape of the incident spectrum), the total amount of reflection seen depends on the solid angle subtended by the material, $\Omega/2\pi = f_{\text{ref}}$, and its inclination to the line of sight. For an assumed inclination angle of 60° , we derived $f_{\text{ref}} = 0.15$ and 0.28 in GS1826–238 and SLX1735–269, respectively, with an associated iron line EqW of 50 and 39 eV. The line EqW and especially the reflected fraction are significantly lower than the ~ 130 eV and $f_{\text{ref}} = 1$ for an isotropic X-ray source above a flat, infinite disk (George & Fabian 1991; Matt, Perola & Piro 1991).

4.2.2. Accretion Geometry

Both the broad band continuum spectrum, and its variability (e.g. van der Klis 1994; Ford et al. 1999) and the properties of the reflected spectrum (Zycki, Done & Smith 1998, 1999) are very similar to that seen in the LS BH systems, suggesting that the same physical mechanisms operate in a similar accretion geometry. If so, then the hard emission cannot have anything to do with the magnetosphere or the NS surface, and must instead be connected with the accretion flow. Mechanisms suggested for the hard power law in BH systems which can also work in NSs are either an accretion disk corona (magnetic reconnection in flares above a disk), or a hot accretion flow. The lack of a strong reflection signature and weak soft emission is at first sight incompatible with the magnetic flaring model. A geometry where the hard X-ray source is above an optically thick disk should lead to $f_{\text{ref}} \sim 1$ rather than the $f_{\text{ref}} \lesssim 0.3$ observed here. In addition, of the hard X-ray flux, half will go up and escape while half will go down and illuminate the cool material. Of these, 10% can be reflected as a hard X-ray component (if the material is mostly neutral, and has solar abundances), but the remaining 90% are thermalised, and should emerge as a soft component. The soft photon luminosity would then be roughly half of that of the hard component. However, it is only emitted into 2π solid angle because it is optically thick, and since the hard component is emitted into 4π ; the inferred luminosities of the soft and hard compo-

nents should be about equal (see Gierlinski et al. 1997).

The properties of the reflected component and line emission together with the observation of time smearing or delays in the optical counterparts of X-ray bursts testify of the presence of an outer disk in those systems. It would seem however that a significant fraction of the disk cannot be seen, either in reflection, or by reprocessing the hard X-ray radiation, or by emission. So the question is: is there then an inner disk at all, say within $\sim 50 - 100 R_S$? If not, then the disk corona model can be ruled out. However, the disk reflection and reprocessing signatures could perhaps be masked by a very highly ionised inner disk (Ross et al. 1998, but see Done & Zycki 1998), while the intrinsic disk emission is then cooler and less intense if the power is mostly dissipated in the corona (Svensson & Zdziarski 1994). Another possibility is that the hot plasma has a bulk velocity βc directed away from the disk (Beloborodov 1999). The bulk motion might be due to the pressure of the reflected radiation and/or plasma ejection from magnetic flares. A mildly relativistic escaping flow ($\beta \sim 0.3$) causes aberration which reduces the downward irradiating flux which in turn reduces the feedback of reflection and reprocessing.

Perhaps the most telling discrepancy in all these models is that there should also be strong emission from a boundary layer where the disk and NS interact. The boundary layer emission can be twice as large as that from the accretion disk (whether standard disk or disk powered corona) once relativistic corrections are included (Shakura & Sunyaev 1986). There is no strong soft emission component in the spectrum, ruling out an optically thick boundary layer (unless it also dissipates most of the accretion energy in an optically thin region perhaps powered by magnetic reconnection). King & Lasota (1987) calculated that the boundary layer between a standard disk and the NS can be optically thin only for mass accretion rates much lower than those considered here (but see recent calculations by Inogamov & Sunyaev, 1999 and Popham & Sunyaev 1999). Alternatively, if the disk truncates at the last stable orbit (allowed only for certain NS equations of state) then the boundary layer is between material freely spiraling in rather than a disk. This can give an

optically thin boundary layer up to luminosities of a few percent of Eddington, as required here (Kluźniak & Wilson 1991). However, it seems unlikely that an optically thin, hot boundary layer could be similar in temperature and variability to disk emission produced by a completely different process of magnetic flare. Removing the boundary layer by ejecting the material just before it reaches the NS surface (e.g. by a centrifugal magnetic field barrier or winds) is not a viable way around these difficulties. The observation of X-ray bursts from these systems proves that the accreting material does accumulate on the NS surface (e.g. GS1826–238).

Such a series of requirements make the disk corona models seem rather contrived, so we investigate the alternative model where the inner disk is replaced by an X-ray emitting hot flow. This would naturally account for the weakness of reflection and reprocessing, and the relative weakness of the intrinsic soft emission. It also provides an explanation for the strong correlation observed between the relative strength of the reflection component (f_{refl}), and the photon index of the intrinsic PL (Γ) in Seyfert galaxies and galactic BHs (Zdziarski et al. 1999). The same correlation also applies to NSs, including those considered here; for GS1826–238, $f_{\text{refl}}=0.15^{+0.03}_{-0.04}$ and $\Gamma=1.72^{+0.01}_{-0.01}$, whereas for SLX1735–269, the corresponding values are $f_{\text{refl}}=0.28^{+0.09}_{-0.12}$ and $\Gamma=2.09^{+0.03}_{-0.04}$. This correlation can be understood by considering a hot X-ray plasma that fills a variable-radius hole in the inner disk; as the disk radius decreases, its solid angle increases, thereby increasing both the reflection and the flux of cool cooling photons. The stronger cooling of the hot plasma then leads to a steepening of the PL slope (Zycki, Done & Smith 1998, Zdziarski et al. 1999)⁸.

The above scenario, where the innermost radius

⁸Alternatively, this correlation can also be explained by the outflow model of Beloborodov (1999). Increasing the semi-relativistic outflow velocity, β , leads to a decrease of both Γ and f_{refl} , and yields a correlation that seems to fit better the observations than the two phase disk model (Zdziarski et al. 1999). Another interesting feature of the ejection model, is that it can explain $f_{\text{refl}} \gtrsim 1$ (as observed in some Seyferts) because for negative values of β , the coupling between the ejected plasma and the disk can be very strong. As said above, however, the weak point of such a model is that it relies on the poorly known physics of the magnetic dissipation within the disk.

of the accretion disk moves as a function of spectral state, can also naturally explain the strong correlation between spectral properties and the frequency of the HFQPOs (e.g. Kaaret et al. 1998; Mendez et al. 1999, Bloser et al. 1999). While there are several current models proposed for these high frequency features in the power spectrum, they all require that the NS spin beats with an inner disk frequency (see e.g. the review by Van der Klis 1998). The easiest way to change the inner disk frequency is to change the inner disk radius. This then naturally explains the lack of HFQPOs in the LS NSs as being systems where the inner disk is truncated at large radii, where the interaction with the NS surface is small. As the disk moves inwards, the spectrum softens (Γ increases; e.g. in 4U0614+09 and 4U1608-52, Kaaret et al. 1998, and the disk contribution increases; e.g. 4U0614+09, Ford et al., 1997), the HFQPOs appear, and their frequencies increase (Piraino et al., 1999).

How can we reconcile our spectral and timing observations in that picture? GS1826–238 would have an accretion disk with a large inner radius. Its inner disk temperature is then too low for its contribution to be detected with the PCA. The cooling is low, its spectrum is hard and the amount of reflection is rather small. Conversely, for SLX1735–269, the disk extends closer to the irradiating source, the solid angle for reflection is larger and its spectrum is softer. Finally for KS1731-260, the disk gets even closer; kilo-Hz QPOs are produced and are seen before disappearing as a response to a further increase of the accretion rate. The cooling is strong and leads to a quenching of the hard X-ray emission; at the same time the iron line gets stronger (so probably, does the reflection component). The above picture, although attractive, does not explain why 1E1724–3045, which has spectral and timing parameters more or less similar to SLX1735–269 does not display any reflection component (yet it shows a weak iron line). One possible explanation could be that the inclination is larger for 1E1724–3045 than for SLX1735–269.

4.2.3. Emission Mechanisms

But what can replace the inner accretion disk? The recent rediscovery of a stable, X-ray hot solution of the accretion flow equations has caused

much excitement. The main assumption of these advective solutions is that the gravitational energy released by viscosity is gained mainly by the protons, and that these heat the electrons only by Coulomb collisions. For low mass accretion rates the flow is optically thin so that the Coulomb collision rate is very low. The proton temperature is high, so the flow has a large scale height (quasi-spherical). The small amount of energy that is gained by the electrons is radiated as cyclo/synchrotron emission, bremsstrahlung and Comptonization of these seed photon distributions (Narayan & Yi 1995). Pure advective models have a disk existing only at very large radii, where its emission is negligible. The resulting spectrum is then rather hard, since the only seed photons are the self-produced ones in the optically thin flow, and the electron temperature is of order ~ 100 keV (Narayan & Yi 1995). As the mass accretion rate increases, the flow becomes denser, so the Coulomb collisions are more effective at transferring energy from the protons to the electrons, so the radiative efficiency increases. But this process cannot continue indefinitely: as the flow becomes optically thick, the Coulomb collisions drain all the energy from the protons, and the flow collapses into a standard, optically thick, geometrically thin accretion disk (Esin et al. 1998).

However, there is a clear difference between advective models for BH and NS systems. For BHs the energy advected with the protons in the flow can be swept invisibly down into the black hole. Such a flow will collapse at $L \sim 0.4\alpha^2 L_{\text{Edd}}$ where $\alpha \sim 0.2$ (Yi et al. 1996) is the α disk viscosity. For NSs the advected energy is released in a boundary layer as the flow hits the NS surface. If this boundary layer is optically thick, then the increase in seed photons for the Compton cooling will cause the advective flow to collapse at Eddington scaled mass accretion rates lower (by at least a factor 3) than for BHs (Narayan & Yi 1995; Yi et al. 1996). Yet the spectral state transition takes place at roughly the same Eddington fraction for NSs and BHs, namely at $\sim 0.05 - 0.1 L_{\text{Edd}}$ (see e.g. Mitsuda et al. 1989 for the NS 4U1608-52, and for the BH Cyg X-1, Esin et al. 1998, see also Esin et al. 1997), and no strong soft emission from a boundary layer is seen.

One way out of this impasse is if the boundary layer is optically thin. Explicit calculations

for the boundary layer between an ADAF and NS surface have not yet been done, though rather different spherical flows have been shown to give optically thin boundary layer emission up to fairly high luminosities (e.g. Zane et al. 1998). Thus an optically thin boundary layer between an advective flow and NS seems plausible. In this case, the boundary layer is an additional heating source for the hot plasma in the advective flow, so it might be expected to merge rather smoothly in both spectral and variability properties with the rest of the hot, optically thin accretion flow. The extra photons from the boundary layer are then hard. This lowers the temperature of the advective flow slightly, but the critical mass accretion rate which can be sustained in the flow is then very similar to that calculated for the BH case (Narayan & Yi 1995). The one caveat to this is that even if the boundary layer were optically thin then the NS surface would intercept and thermalize some of the boundary layer emission, again leading to an additional source of soft seed photons. If the NS surface is ionised and/or mainly made up of hydrogen due to settling of heavy elements, then the reflection albedo can be as high as 0.6. Thus at least 25% of the boundary layer luminosity should emerge as a soft component. We are currently calculating the effect of such an optically thin boundary layer plus its thermalized emission on the properties of the advective accretion flow, to see whether it can allow the observed similarity in state transition accretion rate between BHs and NSs (Done & Barret 1999).

It has been recently suggested that mass loss via winds was a natural consequence of ADAFs, and was such, that only a tiny fraction ($\ll 1$) of the gas supplied through the ADAFs was actually accreted onto the central object (Blandford and Begelman 1999, Quataert & Narayan 1999). Such winds would provide an alternative explanation for the dimness of quiescent BHs, attributed in the ADAF models, to low radiative efficiency and the existence of event horizons in those systems (Narayan, Garcia & McClintock 1997; Menou et al. 1999). However, in our picture, where the NS is surrounded by an ADAF, the observation of X-ray bursts tells us that all the matter flowing through the ADAF can be accreted onto the NS. So, unless the mass transfer rate is very much larger than currently thought in LMXBs (see Menou et

al. 1999 for a recent discussion), the presence of ADAFs around bursting NSs would strongly argue against the existence of powerful winds from such accretion flows (i.e. ADIOS in Blandford & Begelman 1999).

To summarize, the similarity of the BH and NS spectra and variability in their LS strongly suggest that the same mechanisms are operating i.e. that the hard X-ray emission is connected to the accretion flow with the NS surface having little impact on it. Although the latter remains an unescapable part of the system, there is nothing which can be firmly associated with the strong emission expected from the surface or the boundary layer even though it is known that the accretion material has to accumulate onto the NS surface because of X-ray bursts. This problem applies to both the disk corona and advective flow models. The boundary layer emission then must either be optically thin, or emitted at too low a temperature to be observed. The latter seems unlikely given previous ASCA and *Beppo-SAX* observations, hence we conclude that the boundary layer is optically thin, and hot (see recent calculations by Popham & Sunyaev, 1999, Inogamov & Sunyaev, 1999). However, it seems difficult to imagine a situation where the boundary layer emission could have similar spectral and variability properties to magnetic flares above a disk. Hence we favor models where the inner disk is replaced by an X-ray hot, optically thin flow. The only known stable hot solutions to the accretion equations are the advective flows. Unfortunately ADAF solutions have not been developed with self-consistency for the NS case, and it is not yet known whether these can have an optically thin boundary layer. If so then this emission could well merge smoothly with the hot optically thin advective flow. We stress that the maximum mass accretion rate at which an advective flow can be sustained holds out the possibility of showing whether or not advective flows can really be present. Observations show that the hard/soft spectral transition associated in these models with the collapse of the advective flow occurs at roughly the same mass accretion rate in both NS and BH systems. While an optically thick boundary layer produces a large difference in this critical mass accretion rate, an optically thin boundary layer does not. However, even an optically thin boundary layer produces some soft

photon flux from reprocessing of the flux illuminating the NS surface, which will lower this critical mass accretion rate. Further calculations are needed to see whether this effect is small enough to match the observed spectral transitions in NSs.

4.3. Comparison between BHs and NSs

Thanks to RXTE and *Beppo-SAX*, the number of LS NSs observed simultaneously in X-rays and hard X-rays is growing rapidly, so that reliable comparisons between BHs and NSs can now be carried out. Although, as illustrated in this paper, the most recent data indicate that BHs and NSs are very similar in many respects, especially in their low states, it remains critical to search for observational criteria that could distinguish these two types of accreting systems.

4.3.1. Spectral shape differences?

Heindl & Smith (1998) have pointed out that the index of the power law part of the spectrum is significantly larger for NSs than for BHCs ($\Gamma \gtrsim 1.8$ for NSs versus $1.4 \lesssim \Gamma \lesssim 1.6$ for BHs, see however Churazov et al. 1997 for an opposite conclusion). The data presented here are in general terms consistent with this claim, but indicates that the separation is by no means large (the index for GS1826-238 is 1.7). On the other hand, Heindl & Smith's claim, is inconsistent with several recent observations of NSs, as for example those of SAXJ1748.9-2021 in NGC 6440 (In't Zand et al. 1999) or those of the two dippers 4U1915-05 (Church et al. 1998) and XB1323-619 (Balucinska-Church et al., 1999). In the first case, a fit by a broken PL yields a photon index of 1.54 ± 0.03 and 2.13 ± 0.04 below and above the break at 18.1 ± 1.2 keV (In't Zand et al. 1999). For 4U1915-05, the broad band 0.2-200 keV non-dip *Beppo-SAX* spectrum can be fitted by a blackbody plus a cutoff PL of index 1.6 ± 0.01 ($E_{\text{Cutoff}} = 80.4 \pm 10$ keV). Similarly, for XB1323-619, Balucinska-Church et al. (1999) have found that the non-dip spectrum is a cutoff power law with $\Gamma = 1.48 \pm 0.01$ and $E_{\text{Cutoff}} = 44.1$ keV. Based on these observations, we therefore conclude that the above criterion is not valid.

It has also been proposed that, in the framework of thermal Comptonization models, the electron temperature of the scattering cloud (kT_E) appeared to be systematically lower for NSs than for

BHs; $kT_E \lesssim 30$ keV versus $kT_E \gtrsim 50$ keV (Tavani & Barret 1997, Zdziarski et al., 1998, Churazov et al. 1997). This naturally reflects the standard picture that on average BH spectra are harder than NS spectra, and has been tentatively explained by the additional cooling provided by the NS surface, which may act as a thermostat capable of limiting the maximum kT_E achievable in these systems (Kluźniak 1993, Sunyaev and Titarchuk 1989). The data presented in this paper are certainly consistent with this criterion. However, it is worth noting that there are some speculative BHCs (e.g. GRS1758-258) for which kT_E derived from the fitting of their hard X-ray spectra with the Sunyaev & Titarchuk (1980) Comptonization model (*Compst* in XSPEC) is below 50 keV ($kT_E \sim 33$ keV in Mandrou et al. 1994 from a fit of SIGMA data alone). However, as pointed out by Zdziarski et al. (1998), the latter temperature is probably a gross underestimate, and should be reevaluated using broad band spectra and more appropriate relativistic Comptonization models including Compton reflection and relativistic effects (e.g. Poutanen & Svensson 1996). If such an underestimate has indeed been observed in Cyg X-1 (kT_E increased from 27 keV with *Compst* up to ~ 100 keV with *CompPS*; Gierlinski et al. 1997), we note that in the case of 1E1724–3045, kT_E derived with *Compst* is 30 keV, whereas it is only slightly larger (~ 35 keV) with the relativistic *CompPS* model (the same is true for GS1826–238). Bearing this in mind, it remains that this criterion should be considered seriously for sources showing evidence for thermal cutoffs in their hard spectra. More data should tell us soon whether all BHCs fitted with relativistic Comptonization models will indeed have $kT_E \gtrsim 50$ keV, whereas all NSs fitted with the same models will have kT_E below the above value.

In any case, the above criterion applies when an energy cutoff is observed. However such cutoffs are not always present in NS hard X-ray spectra. The first SIGMA observation of 1E1724–3045 revealed a non attenuated hard power law ($\Gamma=1.8$) extending up to 200 keV (Barret et al. 1991). Aql X-1 was also observed by BATSE from 20 keV up to ~ 100 keV with Γ in the range 2.1-2.6 and no evidence for a high energy cutoff (Harmon et al. 1996). Finally, a recent *Beppo-SAX* observation of 4U0614+09 has placed a lower bound on

any exponential cutoff of the power law ($\Gamma=2.3$) of 200 keV⁹ (Piraino et al. 1999). This means that just as there are two classes of BHs based on their hard X-ray spectra (Grove et al. 1998), there might also be two classes of NSs. Members of the first class would display hard X-ray spectra with energy cutoffs, which would result from thermal Comptonization. Members of the second class would have non-attenuated power laws (up to an energy which remains to be accurately determined), similar to the power laws observed in the soft state of BHs. Such power laws could be produced by non-thermal Comptonization, i.e. Comptonization on non-thermal particles (for recent reviews see Poutanen 1999, and Coppi 1999). Alternatively, Titarchuk et al. (1997) have proposed that these power laws could be produced by bulk-comptonization in a convergent accretion flow. The same mechanism seems to be ruled out for NSs because it produces spectra much harder than that observed ($\Gamma \lesssim 1$, Titarchuk et al. 1996). BHs with power laws have typical Γ in the range 2.5-3.0, or similar to NSs in the hard X-ray band (e.g. 1E1724–3045). Therefore, the indication of a steep hard X-ray ($E \gtrsim 30$ keV) spectrum with $\Gamma \gtrsim 2.5$ cannot alone be used to claim that an unknown system contains a NS. Similarly, a hard X-ray power law spectrum with $\Gamma \lesssim 2.5$ is not unique to BHs (e.g. 4U0614+091).

4.3.2. Luminosity differences?

The idea that BHs and NSs are actually hardly distinguishable by their broad band spectral shape has led Barret et al. (1996) to propose a luminosity criterion (see also Barret & Vedrenne 1994, Van der Klis & Van Paradijs 1994). They compared the 1-20 keV luminosity ($L_{1-20 \text{ keV}}$) to the 20-200 keV luminosity ($L_{20-200 \text{ keV}}$) for all secure BHBs (by secure we mean BHs with mass function estimates indicating a compact object of mass larger

⁹Alternatively, the *Beppo-SAX* spectrum could be modeled as thermal Comptonization (*CompPS* model in XSPEC, Poutanen & Svensson, 1996) for which a very high kT_E was derived (246_{-30}^{+50} keV, Piraino et al. 1999). Such a value, which puts the cutoff energy above 700 keV, is itself well above the high energy threshold of the *Beppo-SAX*/PDS (the last significant data point of the spectrum is at 180 keV), and therefore must be considered with cautions. However, if this result is confirmed by observations performed at even higher energies, it would make the kT_E criterion discussed above definitely invalid.

than $3M_{\odot}$, hereafter BHBs for BH Binaries), and all NSs detected up to at least 100 keV. Figure 13 is an updated version of Fig. 1 in Barret et al. (1996). There are now 16 NSs detected at 100 keV with (quasi-)simultaneous coverage in X-rays; all but Cen X-4 detections came within the last 8 years. It includes 6 more NSs recently detected by either RXTE (PCA+HEXTE) or *Beppo-SAX* (MECS+LECS+HPGSPC+PDS); namely the millisecond pulsar SAXJ1808.4-3658 (Gilfanov et al. 1998, Heindl & Smith 1998), the dippers 4U1915-05 (Church et al. 1998) and XB1323-619 (Balucinska-Church et al., 1999), SAXJ1748.8-2021 (In't Zand et al. 1999), SLX1735-269 and GS1826-238 (this work). For the two dippers, $L_{1-20 \text{ keV}}$ and $L_{20-200 \text{ keV}}$ have been computed from their non-dip spectra. In addition, the luminosities for 1E1724-3045 (this work), for 4U0614+091 (*Beppo-SAX* observation, Piraino et al. 1999), and Aql X-1 (joint nearly simultaneous BATSE & ASCA observations, Rubin et al. 1999) have been updated. The figure also includes GRS1009-45 (Nova Velorum 1993), recently shown to be another secure BHB (Filippenko et al. 1999).

For both SAXJ1808.4-3658 and 4U1915-05, we have assumed the distance inferred from X-ray burst studies: 4 and 9.3 kpc respectively (In't Zand et al. 1998, Yoshida 1992), and for XB1323-619 a distance of 10 kpc (Balucinska-Church et al., 1999). SAXJ1748.8-2021 is located in the globular cluster NGC6440 whose distance is estimated to be 8.5 ± 0.5 kpc (Ortolani et al. 1994). For GRS1009-45 we have estimated the distance according to the method described in Barret et al. (1996). We determine the radius of the secondary assuming that it fills its Roche lobe (the radius is then given by the orbital period $P_{\text{orb}}=6.86$ hours, and its mass, which we take to be $0.5 M_{\odot}$). For a K7 secondary, from the absolute visual flux, we determine the absolute visual magnitude $M_v \sim 8.2$, according to the values tabulated by Popper (1980). Finally, using the apparent dereddened magnitude corrected for interstellar reddening and for the contribution (fdisk) by the accretion disk to the continuum flux ($V_{\text{quies}} = 21.4 - 21.9$, $E(B-V)=0.2$, fdisk=60%, Shahbaz & Kuulkers 1998), we obtain a distance in the range 5.0 to 6.5 kpc. Shahbaz and Kuulkers (1998) using an empirical linear relationship between the orbital period, the optical outburst amplitude magnitude derived a

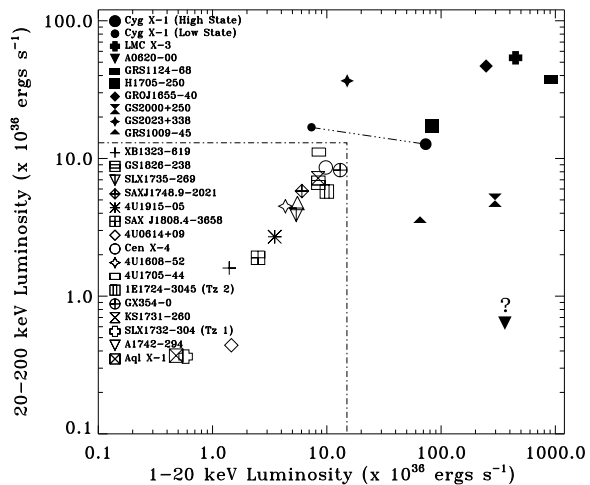


Fig. 13.— The hard X-ray (20-200 keV) versus the X-ray (1-20 keV) luminosities of Black Hole Binaries (filled symbols) and Neutron Star Binaries (open symbols). Only BHs with mass functions indicating a mass for the compact object in excess of $3M_{\odot}$ are considered. For NSs, the luminosities are computed from observations in which the source was detected up to at least 100 keV. For KS1731-260, the luminosities drawn correspond to the SIGMA detection (Barret et al. 1992). This is an updated version of Fig. 1 in Barret et al. (1996) from which most luminosities can be retrieved. The so-called *X-ray burster box* is plotted as a dot-dashed line. Its boundaries are simply defined as to contain all the NSs.

distance of 4 kpc. We adopt in Fig. 13 a distance of 5 kpc. The X-ray and hard X-ray fluxes for GRS1009-45 have been taken from Barret et al. (1996) from observations reported by Sunyaev et al. (1994).

Looking at Fig. 13, one can see that the distinction in luminosity clearly holds: all NSs lie in the so-called *X-ray burster box*, whereas all BHBs are found outside. This figure shows that comparisons of $L_{20-200 \text{ keV}}$ and $L_{1-20 \text{ keV}}$ can be used to distinguish between BHBs and NSs. First, although the presence of a hard tail is not a unique signature of BH accretion, the high luminosity in the hard tail appears to be such a signature: only BHBs are observed with $L_{20-200 \text{ keV}} \gtrsim L_{\text{crit}}$, where we define $L_{\text{crit}} \sim 1.5 \times 10^{37} \text{ ergs s}^{-1}$. Second, the hard X-ray luminosity of NSs can approach L_{crit} , but only

when $L_{1-20 \text{ keV}} \lesssim L_{\text{crit}}$. On the other hand BHBs can have both $L_{1-20 \text{ keV}}$ and $L_{20-200 \text{ keV}}$ above L_{crit} (although $L_{20-200 \text{ keV}}$ may then be substantially lower than $L_{1-20 \text{ keV}}$). Finally, the most recent broad band measurements of LS NSs as those presented in this paper all indicate that these systems have a ratio $L_{1-20 \text{ keV}}/L_{20-200 \text{ keV}}$ in a narrow range of $\sim 1.0 - 2.0$. This yields the correlation between $L_{1-20 \text{ keV}}$ and $L_{20-200 \text{ keV}}$ seen in Fig. 13. This suggests that below a luminosity $\sim 2 \times L_{\text{crit}}$, the spectral shape of a given NS does not depend much on its luminosity. However, observation of softer spectra (almost blackbody-like, Asai et al. 1998) from quiescent NS transients imply that this correlation breaks down somewhere between $\sim 10^{34}$ and 10^{36} ergs s^{-1} . Another interesting feature of Fig. 13 is the fact that the BHBs (those lacking an ultra soft component) lie roughly on an extrapolation of the sequence formed by the NSs points. This again points to the underlying similarity of their emission sources and basic accretion geometries.

5. Summary

We have reported RXTE timing and spectral observations of four type I X-ray bursters. The results presented here nicely illustrate that beside its unprecedented timing capabilities, RXTE has also sufficient sensitivity for detailed spectral studies. Our spectral fitting has revealed that the broad band spectra of low state NSs are often more complicated than previously thought. In particular, we have detected a Compton reflected component plus an iron $K\alpha$ line in two systems. In both cases, the data indicate that the most likely site for the reflector is a cool accretion disk, which is truncated somewhere to offer a relatively small solid angle to the irradiating source, which could be a quasi-spherical hot advection dominated inner accretion flow. Similar behavior is observed among BHs leading to very similar conclusions. In addition, within the limitations of the PCA calibration uncertainties at low energies, we have detected a soft component, which is equally well described by a multi-color disk blackbody or a blackbody. In our picture, this soft component most probably originates from the truncated accretion disk.

At higher energies, the HEXTE sensitivity is sufficient to accurately locate the energy cutoff in

the low state hard X-ray spectra of these systems. When combined with PCA data, we have shown that the spectral steepness of the hard tails observed by SIGMA/BATSE was not intrinsic, but was rather due to the presence of a high energy cutoff ($\sim 50 - 80$ keV). The cutoff power law spectral shape observed strongly suggests that thermal Comptonization is the dominant emission mechanism in these systems. The Comptonization process would take place in an optically thin hot boundary layer merged with the central advective corona, located between the truncated accretion disk and the NS surface.

Of the most recent criteria that have been proposed to distinguish BHs from NSs (out of quiescence), two appear consistent with all the available data. The first one states that for NSs displaying thermal Comptonization, they seem to be unable to achieve electron temperature as high as BHs, and hence Comptonization with $kT_E \gtrsim 50$ keV would be a BH signature. This criterion is weakened however by the fact that there are some NSs that do not display high energy cutoffs in their hard X-ray spectra. The second one is a luminosity based argument and claims that only BHs are capable of emitting bright hard X-ray tails with luminosity larger than $\sim 1.5 \times 10^{37}$ ergs s^{-1} .

The RXTE archive contain a wealth of observations of NSs and BHs in different luminosity states, and represent a very uniform data set, that should be used to test the picture proposed in this paper. It is also clear that the same data can be used to challenge the observational criteria discussed above to distinguish BHs from NSs.

6. Acknowledgments

This research has made use of data obtained through the High Energy Astrophysics Science Archive Research Center operated by the NASA Goddard Space Flight Center. GKS is grateful to CESR for its hospitality during the period of this work. DB wishes to thank the organizers of 1999 ITP Black Hole Program (R. Blandford, D. Eardley, and J.P. Lasota) and the participants (R. Taam, S. Kato, A. Zdziarski, P. Coppi and O. Blaes) and for their hospitality at the Institute of Theoretical Physics where part of this work was completed. DB acknowledges many exciting discussions with all of them. This research was

thus supported in part by the National Science Foundation under Grant No. PHY94-07194. DB also thanks the organizers of the Aspen Center for Physics summer workshop on “X-Ray Probes of Relativistic Effects near Neutron Stars and Black Holes” (J.E. Grindlay, P. Kaaret, W. Kluzniak, F. Lamb, M. Nowak, W. Zhang) for inviting him, and for their hospitality during the workshop.

The authors are grateful to J. Swank and K. Jahoda for discussions about the PCA calibrations, to L. Titarchuk for useful discussions during his stay at CESR, to A. Zdziarski for providing us with the GINGA spectrum of GS1826–238, to J. Poutanen for the supply of his relativistic Comptonization model (*CompPS*), and finally to P. Kaaret for sending us in advance a copy of the paper Piraino et al. (1999) on 4U0614+09.

This paper greatly benefited from many useful comments by A. Bazzano, P.F. Bloser, E.C. Ford, M. Guainazzi, P. Kaaret, W. Kluzniak, J.P. Lasota, J.E. McClintock, J. Poutanen, R. Taam, M. Van der Klis, A. Zdziarski, S.N. Zhang, and W. Zhang.

Finally, we are thankful to Dimitrios Psaltis, the referee, for many insightful and thoughtful comments on this paper.

REFERENCES

- Aleksandrovich, N. L, et al., 1995, *Sov. Astr. Lett.*, 21, No 3, 431
- Arnaud, K.A., 1996, *Astronomical Data Analysis Software and Systems V*, eds. Jacoby G. and Barnes J., ASP Conf. Series vol 101, 17
- Asai, K., et al., 1998, *PASJ*, 50, 611
- Balucinska-Church, M., et al., 1999, *A&A*, 349, 495
- Barbuy, B., Bica, E. & Ortolani, S. 1998, *A&A*, 333, 117
- Barret, D., et al., 1999a, *A&A*, 341, 789
- Barret, D., et al., 1999b, *Adv. in Space Res.*, in press
- Barret, D., Motch, C., & Predehl, P., 1998, *A&A*, 329, 965
- Barret, D., McClintock, J. E., & Grindlay, J. E. 1996, *ApJ*, 473, 963
- Barret, D., Motch, C., & Pietsch, W., 1995, *A&A*, 303, 526
- Barret, D. & Vedrenne, G., 1994, *ApJS*, 92, 505
- Barret D., et al., 1992, *ApJ*, 394, 615
- Barret, D., et al. 1991, *ApJ*, 379, L21
- Bazzano, A., et al., 1997, *IAU Circ.*, 6668
- Bazzano, A., et al., 1997, *Proc. of the Fourth Compton Symposium*, Eds. C. Dermer, M.S. Strickman, J.D. Kurfess, AIP Conf. Proc. 410, 729
- Beloborodov, A. M. 1999, *ApJ*, 510, L123
- Blandford, R. D. & Begelman, M. C., 1999, *MNRAS*, 303, L1
- Bloser, P. F., et al., 1999, *ApJ*, submitted
- Bradt, H. V., Rothschild, R. E. & Swank, J. H., 1993, *A&AS*, 97, 355
- Brainerd, J. & Lamb, F. K. 1987, *ApJ*, 317, L33
- Churazov, E., et al., 1997, *Advances in Space Research*, 19, 55
- Church, M. J., et al., 1998, *A&A*, 338, 556
- Coppi, P., 1999, in *High Energy Processes in Accreting Black Holes*, Eds. J. Poutanen, R. Svensson, ASP Conf. Proc., Vol 161, 375
- Cui, W., et al. 1998, *ApJ*, 502, L49
- David, P., et al., 1997, *A&A*, 322, 229
- De Jong, J.A., Van Paradijs, J. & Augusteijn, T. 1996, *A&A*, 314, 484
- Del Sordo, S. et al., 1999, in press
- Done, C. & Barret, D., 1999, *ApJ*, in preparation
- Dubus, G. et al., 1999, *MNRAS*, 303, 139
- Ebisawa, K. , et al. 1994, *PASJ*, 46, 375
- Elvis, M. et al., 1992, *ApJS*, 80, 257
- Esin, A., et al., 1998, *ApJ*, 505, 854
- Esin, A., McClintock, J.E., R. Narayan, 1997, *ApJ*, 489, 865

- Filippenko, A. et al., 1999, PASP, 111, 969
- Ford, E. C., et al., 1999, ApJ, 512, L31
- Ford, E. C., et al., 1998, ApJ, 498, L41
- Ford, E. C., et al., 1997, ApJ, 486, L47
- Frontera et al., 1998, in “The Active X-ray Sky”,
Eds. L. Scarsi, H. Bradt, P. Giommi, & F.
Fiore, Nuclear Phys. (Proc. Suppl), 69/1-3, 286
- George, I. M. & Fabian, A. C., 1991, MNRAS,
249, 352
- Gierlinski, M. , et al., 1999, MNRAS, in press.
- Gierlinski, M. , et al., 1997, MNRAS, 288, 958
- Gilfanov, M. et al., 1998, A&A, 338, L83
- Goldwurm, A., et al., 1996, A&A, 310, 857
- Goldwurm, A., Denis, M., Paul, J. et al., 1995,
Adv. Spa. Res., 15, 41
- Goldwurm, A., Cordier, B., Paul, J. et al., 1993, in
N. Fichtel, C. and Gehrels and J. Norris (eds.),
The Second Compton Symposium, AIP No. 304,
p. 421
- Grove, J. E., et al., 1998, ApJ, 500, 899
- Grebenev, S. A., Pavlinsky, M. N., Sunyaev, R. A.,
1996, “The 2nd INTEGRAL Workshop: The
Transparent Universe”, St Malo, 16-20 Sep.
1996, 183
- Guainazzi, M., et al., 1998, A&A, 339, 802
- Hanawa, T., 1991, ApJ, 373, 222
- Harmon, B. A. et al., 1996, A&AS, 120, C197
- Hasinger, G. & Van Der Klis, M., 1989, A&A, 225,
79
- Homer, L., Charles, P. A., & O’Donoghue, D.,
1998, MNRAS, 298, 497
- Hua, X., Kazanas, D. & Cui, W., 1999, ApJ, 512,
793
- Kaaret, P., et al., 1998, ApJ, 497, L93
- Inogamov, N. & Sunyaev, R.A., 1999, A&A, sub-
mitted
- Kazanas, D., Hua, X. & Titarchuk, L., 1997, ApJ,
480, 735
- King, A. R. & Lasota, J. P. 1987, A&A, 185, 155
- Kluzniak, W., 1998, ApJ, 509, L37
- Kluzniak, W., 1993, A&AS, 97, 265
- Kluzniak, W. and Wilson, J. R., 1991, ApJL 372,
L87
- Kylafis, N. and Phinney, E. S., 1989, in *Tim-
ing Neutron Stars*, Eds H. Ogelman & E.P.J.
van den Heuvel (NATO ASI), 262, 731 (Dor-
drecht:Kluwer)
- Levine, A. M., et al., 1996, ApJ, 469, L33
- Lochner, J. C., Swank, J. H. & Szymkowiak, A.
E., 1991, ApJ, 376, 295
- Magdziarz, P. & Zdziarski, A., 1995, MNRAS,
273, 837
- Mandrour, P., et al. 1994, ApJS, 92, 343
- Matt, G., Perola, G. C. & Piro, L., 1991, A&A,
247, 25
- Menou, K., 1999, ApJ, 520, 276
- Miller, M. C., Lamb, F. K. & Psaltis, D., 1998,
ApJ, 508, 791
- Mitsuda, K., et al., 1989, PASJ, 41, 97
- Mitsuda, K., Inoue, H., Koyama, K. et al., 1984,
PASJ 36, 741
- Miyamoto, S., et al., 1988, Nature, 336, 450
- Narayan, R. , Garcia, M. R. & McClintock, J. E.
1997, ApJ, 478, L79
- Narayan, R. & Yi, I., 1995, ApJ, 452, 710
- Narita, T. et al., 1999, ApJ, in preparation
- Nowak, M. A., Wilms, J. & Dove, J. B., 1999,
ApJ, 517, 355
- Olive, J. F. & Barret, D., 1999, ApJ, in prepara-
tion
- Olive, J. F., et al., 1999, Advances in Space Res.,
in press

- Olive, J. F., et al., 1998, *A&A*, 333, 942
- Ortolani, S., Bica, E., and Barbuy, B., 1997, *A&A* 326, 620
- Ortolani, S., Barbuy, B. & Bica, E., 1994, *A&AS*, 108, 653
- Paul, J., et al., 1991, *Advances in Space Research*, 11, 289
- Piraino, S. et al., 1999, *A&A*, 349, L77
- Popham, R. & Sunyaev, R. A., 1999, *A&A*, in preparation
- Popper, D. M. 1980, *ARA&A*, 18, 115
- Poutanen, J., 1999, in *Theory of Black Hole Accretion Disks*, Eds, M.A. Abramowicz, G. Björnsson, J.E. Pringle, Cambridge: CUP, 100.
- Poutanen, J. & Fabian, A. C. 1999, *MNRAS*, 306, L31
- Poutanen, J. & Svensson, R. 1996, *ApJ*, 470, 249
- Predehl, P. & Schmitt, J.H.M.M., 1995, *A&A*, 293, 889
- Psaltis, D., Belloni, T. & Van der Klis, 1999, *ApJ*, 520, 262
- Quataert, Eliot & Narayan, Ramesh 1999, *ApJ*, 520, 298
- Rubin, B. et al., 1999b, *Adv. in Space Res.*, in press
- Rothschild, R. E., et al., 1999, *ApJ*, 510, 651
- Rothschild, R. E., et al., 1998, *ApJ*, 496, 538
- Shahbaz, T. & Kuulkers, E., 1998, *MNRAS*, 295, L1
- Shimura, T. & Takahara, F., 1995, *ApJ*, 445, 780
- Skinner, G. K., et al. 1999, *Proc. of the 19Th Texas Symposium*, Paris, in press
- Skinner, G. K., et al. 1987, *Nature*, 330, 544
- Smith, D. A., Morgan, E. H., & Bradt, H., 1997, *ApJ*, 479, L137
- Strickman, M., et al., 1996, *A&AS*, 120, C217
- Sunyaev, R. A., et al. 1994, *Astronomy Letters*, 20, 777
- Sunyaev, R. A. et al. 1990a, *Sov. Astr. Lett.*, 16(1), 59
- Sunyaev, R. A. & Titarchuk, L. G., 1989, in *Proc. of 23rd ESLAB Symposium on two topics in X-ray Astronomy*, J. Hunt & B. Batrick, Eds. (ESA SP-296), p. 627
- Sunyaev, R. A. and Shakura, N. I., 1986, *Sov. Ast. Lett.* 12, 117
- Sunyaev, R. A. & Titarchuk, L. G., 1980, *A&A*, 86, 121
- Svensson, R. & Zdziarski, A. A., 1994, *ApJ*, 436, 599
- Tanaka, Y. 1989, in *Proc. of 23rd ESLAB Symposium on two topics in X-ray Astronomy*, J. Hunt & B. Batrick, Eds. (ESA SP-296), p. 11
- Tavani, M. & Barret, D., 1997, *AIP Conf. Proc. 410: Proc. of the Fourth Compton Symposium*, 75
- Titarchuk, L. & Osherovich, V. 1999, *ApJ*, 518, L95
- Titarchuk, L. , Mastichiadis, A. & Kylafis, N. D. 1997, *ApJ*, 487, 834
- Titarchuk, L., Mastichiadis, A. & Kylafis, N. D. 1996, *A&AS*, 120, C171
- Titarchuk, L., 1994, *ApJ* 434, 570
- Ubertini, P., et al., 1999, *ApJ*, 514, L27
- Ubertini, P., et al., 1997, *IAU Circ.*, 6611, 1
- Valinia, A., & Marshall, F.E., 1998, *ApJ*, 505, 134
- Van der Klis, M. 1997, *The Many Faces of Neutron Stars, Lipari, Italy, October 1-10 (Dordrecht:Kluwer)*
- Van der Klis, M., 1994, *ApJS*, 92, 511
- Van Paradijs, J. & McClintock, J.E., 1994, *A&A*, 290, 133
- Van Paradijs, J. & Van der Klis, M., 1994, *A&A*, 281, L17

- Vikhlinin, A., Churazov, E. & Gilfanov, M. 1994, A&A, 287, 73
- Vrtilek, S. D., et al., M. 1990, A&A, 235, 162
- White, N. E., Stella, L. & Parmar, A. N., 1988, ApJ, 324, 363
- White, N. E., et al., 1986, MNRAS, 218, 129
- Wijnands, R. & Van Der Klis, M., 1999a, A&A, 345, L35
- Wijnands, R. & Van Der Klis, M., 1999b, ApJ, 514, 939
- Wijnands, R. A. D. & Van der Klis, M., 1998, ApJ, 507, L63
- Wijnands, R. A. D. & Van der Klis, M., 1997, ApJ, 482, L65
- Yamauchi, S. & Koyama, K., 1990, PASJ, 42, L83
- Yi, I., et al., 1996, A&AS, 120, C187
- Yoshida, K., Mitsuda, K., Ebisawa, K. et al. 1993, PASJ 45, 605
- Yoshida, K., 1992, PhD Thesis, Tokyo University
- In 't Zand, J. J. M., et al., 1999, A&A, 345, 100
- In 't Zand, J. J. M., et al., 1998, A&A, 331, L25
- In't Zand, J., 1992, PhD Thesis, Utrecht University
- Zane, S., Turolla, R. & Treves, A. 1998, ApJ, 501, 258
- Zhang, S. N. et al., 1996, A&AS, 120C No 4, 279
- Zdziarski, A. A., Lubinski, P. & Smith, D. A., 1999, MNRAS, 303, L11
- Zdziarski, A. A., et al., 1998, MNRAS, 301, 435
- Zycki, P. T., Done, C. & Smith, D. A., 1999, MNRAS, 305, 231
- Zycki, P. T., Done, C. & Smith, D. A., 1998, ApJ, 496, L25